

A comparison of global estimates of marine primary production from ocean color

Mary-Elena Carr^{a,*}, Marjorie A.M. Friedrichs^{b,bb}, Marjorie Schmeltz^a, Maki Noguchi Aita^c, David Antoine^d, Kevin R. Arrigo^e, Ichio Asanuma^f, Olivier Aumont^g, Richard Barber^h, Michael Behrenfeldⁱ, Robert Bidigare^j, Erik T. Buitenhuis^k, Janet Campbell^l, Aurea Ciotti^m, Heidi Dierssenⁿ, Mark Dowell^o, John Dunne^p, Wayne Esaias^q, Bernard Gentili^d, Watson Gregg^q, Steve Groom^r, Nicolas Hoepffner^o, Joji Ishizaka^s, Takahiko Kameda^t, Corinne Le Quéré^{k,u}, Steven Lohrenz^v, John Marra^w, Frédéric Mélin^o, Keith Moore^x, André Morel^d, Tasha E. Reddy^e, John Ryan^y, Michele Scardi^z, Tim Smyth^r, Kevin Turpie^q, Gavin Tilstone^r, Kirk Waters^{aa}, Yasuhiro Yamanaka^c

^aJet Propulsion Laboratory, California Institute of Technology, 4800 Oak Grove Dr, Pasadena, CA 91101-8099, USA

^bCenter for Coastal Physical Oceanography, Old Dominion University, Crittenton Hall, 768 West 52nd Street, Norfolk, VA 23529, USA

^cEcosystem Change Research Program, Frontier Research Center for Global Change, 3173-25, Showa-machi, Yokohama 236-0001, Japan

^dLaboratoire d'Océanographie de Villefranche, 06238, Villefranche sur Mer, France

^eDepartment of Geophysics, Stanford University, Stanford, CA 94305-2215, USA

^fTokyo University of Information Sciences 1200-1, Yato, Wakaba, Chiba 265-8501, Japan

^gLaboratoire d'Océanographie Dynamique et de Climatologie, Univ Paris 06, MNHN, IRD, CNRS, Paris F-75252 05, France

^hDuke University Marine Lab, 135 Duke Marine Lab Rd, Beaufort, NC 28516, USA

ⁱDepartment of Botany and Plant Pathology, Cordley Hall 2082, Oregon State University, Corvallis, OR 97331, USA

^jDepartment of Oceanography, University of Hawaii, Honolulu, HI 96822, USA

^kMax-Planck-Institute for Biogeochemistry, Postfach 100164, D07701 Jena, Germany

^lMorse Hall, University of New Hampshire, 39 College Road, Durham, NH 03824-3525, USA

^mUNESP - Campus do Litoral Paulista, Praça Infante Dom Henrique S/N, São Vicente, São Paulo CEP 11330-900, Brazil

ⁿDepartment of Marine Sciences, University of Connecticut, 1080 Shennecossett Road, Groton, CT 06340, USA

^oJoint Research Center of the E.C., Inland and Marine Waters Unit I-21020, Ispra (Va), Italy

^pNOAA/Geophysical Fluid Dynamics Laboratory, PO Box 308, Forrester Campus B Site, Princeton, NJ 08542-0308, USA

^qNASA Goddard Space Flight Center, Global Modeling and Assimilation Office, Greenbelt, MD 20771, USA

^rRemote Sensing Group, Plymouth Marine Laboratory, Prospect Place, Plymouth, Devon PL1 3DH, UK

^sFaculty of Fisheries, Nagasaki University, 1-14 Bunkyo, Nagasaki 852-8521, Japan

^tGroup of Oceanography, National Research Institute of Far Seas Fisheries, 5-7-1 Shimizu-Orido, Shizuoka 424-8633, Japan

^uUniversity of East Anglia and the British Antarctic Survey, Norwich NR4 7TJ, UK

^vDepartment of Marine Science, 1020 Balch Blvd., Stennis Space Center, MS 39529-9904, USA

^wLamont-Doherty Earth Observatory, 61 Route 9W, Palisades, NY 10964, USA

^xEarth System Science, University of California at Irvine, 3214 Croul Hall, Irvine, CA 92697-3100, USA

^yMBARI, 7700 Sandholdt Rd., Moss Landing, CA 95039-9644, USA

*Corresponding author. Tel.: +1 818 354 5097; fax: +1 818 393 6720.

E-mail address: Mary-Elena.Carr@jpl.nasa.gov (M.-E. Carr).

^zDepartment of Biology, University of Rome 'Tor Vergata', Via della Ricerca Scientifica, 00133 Roma, Italy

^{aa}NOAA Coastal Services Center, 2234 South Hobson Avenue Charleston, SC 29405-2413, USA

^{bb}Virginia Institute of Marine Science, College of William and Mary, P.O. Box 1346, Gloucester Point, VA 23062, USA

Received 2 September 2004; accepted 30 January 2006

Abstract

The third primary production algorithm round robin (PPARR3) compares output from 24 models that estimate depth-integrated primary production from satellite measurements of ocean color, as well as seven general circulation models (GCMs) coupled with ecosystem or biogeochemical models. Here we compare the global primary production fields corresponding to eight months of 1998 and 1999 as estimated from common input fields of photosynthetically-available radiation (PAR), sea-surface temperature (SST), mixed-layer depth, and chlorophyll concentration. We also quantify the sensitivity of the ocean-color-based models to perturbations in their input variables. The pair-wise correlation between ocean-color models was used to cluster them into groups or related output, which reflect the regions and environmental conditions under which they respond differently. The groups do not follow model complexity with regards to wavelength or depth dependence, though they are related to the manner in which temperature is used to parameterize photosynthesis. Global average PP varies by a factor of two between models. The models diverged the most for the Southern Ocean, SST under 10 °C, and chlorophyll concentration exceeding 1 mg Chl m⁻³. Based on the conditions under which the model results diverge most, we conclude that current ocean-color-based models are challenged by high-nutrient low-chlorophyll conditions, and extreme temperatures or chlorophyll concentrations. The GCM-based models predict comparable primary production to those based on ocean color: they estimate higher values in the Southern Ocean, at low SST, and in the equatorial band, while they estimate lower values in eutrophic regions (probably because the area of high chlorophyll concentrations is smaller in the GCMs). Further progress in primary production modeling requires improved understanding of the effect of temperature on photosynthesis and better parameterization of the maximum photosynthetic rate.

© 2006 Elsevier Ltd. All rights reserved.

1. Introduction

Although photosynthesis is a key component of the global carbon cycle, its spatial and temporal variability is poorly constrained observationally. Furthermore it is unclear how this variability may respond to potential scenarios of climate change. Global net primary production, the carbon fixed through photosynthesis and available for higher trophic levels, occurs in both terrestrial (52%) and marine ecosystems (48%) (Field et al., 1998). The highly dynamic nature of marine photosynthesis is revealed by considering that the annual mean value of 45–50 Gt C is carried out by a phytoplankton biomass of ~1 Gt. Ship resources cannot resolve low-frequency spatial and temporal variability, much less make direct observations of mesoscale variability beyond isolated snapshots. The chronic undersampling of ship-based estimates of global primary production requires significant extrapolations, making it essentially impossible to quantify basin-scale variability from in situ measurements.

Fortunately, satellites provide a solution (McClain et al., 1998). Sensors that measure ocean color are

presently used to estimate chlorophyll concentration in the upper ocean. Integrated biomass can be obtained from ocean color by assuming a vertical profile and a carbon to chlorophyll relationship. To go from biomass, a pool, to photosynthesis, a rate, a time dependent variable is needed. Solar radiation is an obvious choice, and simple mechanistic models compute productivity from biomass, photosynthetically available radiation (PAR), and a transfer or yield function which incorporates the physiological response of the measured chlorophyll to light, nutrients, temperature, and other environmental variables. As a variable amenable to remote sensing, sea-surface temperature (SST) is often used to parameterize the photosynthetic potential.

There exist a range of modeling approaches, e.g., Platt and Sathyendranath (1993), Longhurst et al. (1995), Howard and Yoder (1997), Antoine and Morel (1996), Behrenfeld and Falkowski (1997a), or Ondrusek et al. (2001). These models can be distinguished by the degree of explicit resolution in depth and irradiance as described by Behrenfeld and Falkowski (1997b). While vertically and spectrally explicit models incorporate information about algal

physiology and its dependence on environmental factors, the paucity of measurements of physiological characteristics on the global scale hinders their full application. A common parameter in many simpler models is the maximum observed photosynthetic rate (normalized by biomass) within the water column ($P_{\text{opt}}^{\text{B}}$). Another parameter, $P_{\text{max}}^{\text{B}}$, is derived from short-term light-saturated incubations; consequently extant measurements are fewer. $P_{\text{max}}^{\text{B}}$ is defined as the maximum rate of photosynthesis when light is not limiting, while $P_{\text{opt}}^{\text{B}}$ represents the effective photoadaptive yield in the field for specific light conditions.

A series of round-robin experiments have been carried out to evaluate and compare models which estimate primary productivity from ocean color (Campbell et al., 2002). In these experiments, in situ measurements of carbon uptake were used to test the ability of the participating models to predict depth-integrated primary production (PP) based on information accessible via remote sensing. The first round-robin experiment used data from only 25 stations. The second primary production algorithm round robin (PPARR2) used data from 89 stations with wide geographic coverage (Campbell et al., 2002). There were 10 participant teams and 12 models.

Eight models were within a factor of 2.4 (based on one standard deviation in log-difference errors) of the ^{14}C measurements (Campbell et al., 2002). Biases were a significant source of error. If biases were eliminated, 10 of the 12 model estimates would be within a factor of two of the in situ data. The algorithms performed best in the Atlantic region, which has historically contributed the most data for parameterization. The equatorial Pacific and the Southern Oceans presented the worst results. The Southern Ocean data included both the lowest and highest values of primary production, so the poor performance may be related to this dynamic range. The high-nutrient low-chlorophyll (HNLC) conditions observed in both the equatorial Pacific and the Southern Oceans may contribute to the higher model-data misfit, as most models were not developed with data subject to micronutrient limitation. Likewise, globally-tuned parameterizations of temperature and of the vertical extent of surface biomass are likely to fail in both regions.

The third primary production algorithm round robin (PPARR3) compares output from 24 ocean-color-based models and model variants from the US, Europe, Japan, and Brazil (Table 1). The first

Table 1

Model participants, type of model used, group to which they belong, and parts of PPARR3 for which we have received results

No.	Participants	Type	Group	Parts
1	Carr	WIDI	1	1, 2, 3
2	Behrenfeld	WIDI	2	1, 2, 3
3	Behrenfeld	WIDI	4	1, 2, 3
4	Turpie and Esaia	WIDI	2	1, 2, 3
5	Ciotti	WIDI	2	1, 2, 3
6	Ishizaka and Kameda	WIDI	2	1, 2, 3
7	Moore	WIDI	1	1
8	Dierssen	WIDI	1	1, 2
9	Dierssen	WIDI	1	1, 2
10	Dowell	WIDI	2	1, 3
11	Turpie and Esaia	WIDI	4	1, 2, 3
12	Ryan	WIDI	3	1, 2, 3
13	Carr	WIDI	4	1, 2, 3
14	Scardi	WIDI	1	1, 2, 3
15	Lohrenz	WIDR	2	1
16	Lohrenz	WIDR	2	1
17	Lohrenz	WIDR	3	1
18	Asanuma	WIDR	3	1, 2, 3
19	Marra	WIDR	4	1, 2, 3
20	Antoine, Gentili, and Morel	WRDR	4	1, 2, 3
21	Smyth	WRDR	4	1, 2, 3
22	Melin and Hoepffner	WRDR	1	1, 2, 3
23	Waters and Bidigare	WRDR	2	1, 2, 3
24	Arrigo and Reddy	WRDR	4	1, 2, 3
25	Aumont	GCM	5	1, 3
26	Moore	GCM	5	1
27	Yamanaka and Aita	GCM	5	1
28	Dunne	GCM	5	1
29	Buitenhuis and Le Quéré	GCM	5	1, 3
30	Gregg	GCM	5	1
31	Gregg	GCM	5	1

See text for model and group description.

part of PPARR3 is a comparison of monthly global primary production fields generated by the different algorithms while part 2 is a sensitivity analysis. These two parts do not use in situ data to quantify model performance. Therefore, it is not possible to define a 'best' model. Part 3 is a ground-truth comparison like PPARR1 and PPARR2. We compare modeled PP and a high quality database of ^{14}C measurements from the tropical Pacific (Le Borgne et al., 2002). The poor performance of the PPARR2 models in the tropical Pacific and the plentiful high-quality data led us to emphasize this region within PPARR3. An upcoming manuscript (Friedrichs et al., in prep) will present the results of part 3 of PPARR3 and recommend the best performing model for the tropical database comparison. A future study will look at a broader range of in situ data.

Circulation and nutrient fields are necessary to fully quantify oceanic carbon fluxes and biological productivity. In an effort to bring the ocean-color-based productivity modelers together with ecosystem and biogeochemical modelers, we invited the latter group to participate so we can compare their modeled primary production fields for the same time period with those of the ocean-color models. Our sole criterion for participation were that the models simulate global primary production fields.

In this paper, we describe PPARR3 results from parts 1 and 2, i.e. a global intercomparison of models for eight months and a sensitivity analysis. Although a comparison with in situ data is needed to quantify the performance of the models, the intercomparison enables us to discern the conditions under which the models have divergent results. By comparing the model output, we can distinguish groups, which in turn can be understood on the basis of the sensitivity analysis. Here we address the observed spatial, seasonal, and interannual variability among the participating models.

2. Data and methods

2.1. Participating models

The participating models are of all types discussed by Behrenfeld and Falkowski (1997b): wavelength- and depth-integrated (WIDI, 14 models), wavelength-integrated and depth-resolved (WIDR, five models), and wavelength- and depth-resolved (WRDR, five models). The list of models is given in Table 1, classified by model type, with the name of the participant(s), and the PPARR3 parts to which they have contributed. Seven general circulation models coupled to biogeochemistry (GCM-based) have participated in part 1 (global and regional intercomparison). The models are described in the Appendix.

2.2. Approach

The input data required for the participants to estimate integrated primary production were provided by the PPARR3 organizers Carr and Friedrichs; the participants then returned their results for subsequent comparison. In part 1, the input fields corresponded to eight monthly mean global maps of chlorophyll from SeaWiFS, SST from AVHRR Pathfinder, photosynthetically available radiation (PAR) from SeaWiFS, and mixed-layer

depth estimated from two different general circulation models: the JPL-MIT model and the NCAR model. Despite differences in the two fields of mixed-layer depth, the impact on the resulting PP fields was almost negligible. Hereafter, we only show results which used mixed-layer depth from the JPL-MIT model. The monthly means correspond to January, March, May, July, September, November, and December 1998, and December 1999. We worked at a nominal 18-km resolution obtained by subsampling the 9-km standard-mapped-image fields. The participants (Table 1) used these input fields to estimate primary production integrated to the 1% light level (hereafter PP). Here we compare the resulting PP fields. The approach is outlined in Fig. 1 for December 1998. This study does not provide an estimate of the global PP for the study period, but rather compares model output to identify the conditions under which models diverge. In fact we have used Version 2 of SeaWiFS data (first reprocessing), but for our purpose of model intercomparison, improved chlorophyll determination has little bearing except in localized areas. Save two exceptions, the GCM-based models did not use any of the input variables that were so fundamental to the ocean-color-based models. Participation of the GCM modelers was added after the project design was developed. Model #26 used the MLD fields and model #31 assimilated the SeaWiFS chlorophyll, although not the same version and resolution as shown here.

The pair-wise linear correlation of the spatial and seasonal variability of the models enables us to distinguish four groups of ocean-color-based models, within which the models are highly correlated, and among which the correlation is less (see Section 3.1 below). To derive a mean model, we averaged the models within each group together (omitting model #4 because it is identical to model #2) and then averaged the four group-average models together. The model spread is then quantified by comparing each model with the mean model. We calculated the difference between the decimal logarithm (log base 10) of each model and that of the mean, which is in effect the logarithm of the ratio between the model and the average model, following Campbell et al. (2002). We divided the global fields into basins, SST levels, chlorophyll concentrations, and basin-latitudinal bands to evaluate model similarity and divergence. There is no reason to assume that the mean model is closer to truth than the outlier models that appear as

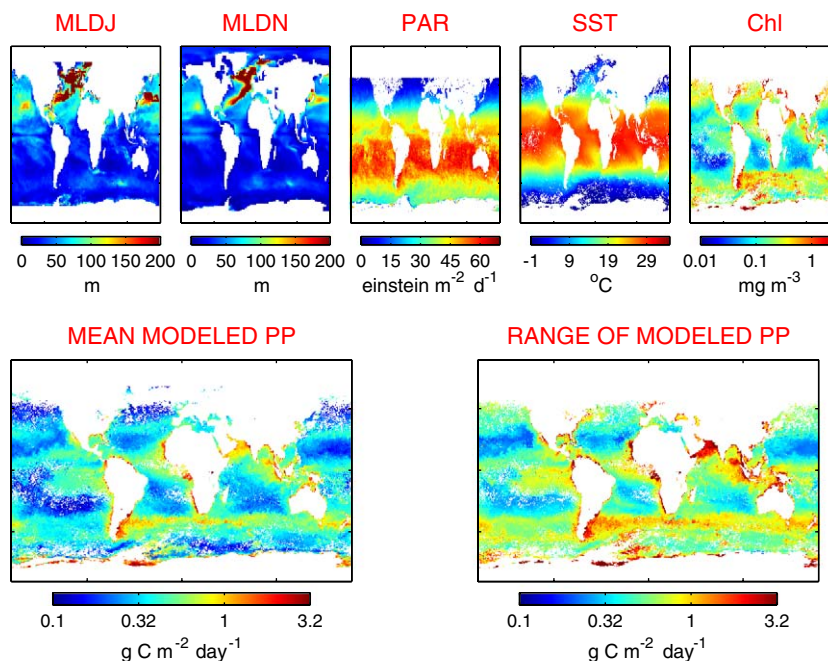


Fig. 1. Approach taken in Part 1 of PPARR3. The ocean-color modelers were given monthly mean input files: mixed-layer depth from two GCMs (MLDJ and MLDN), SST, PAR, and chlorophyll concentration. They estimated integrated primary production and returned their values to the organizers. These are the input fields corresponding to January 1998 and the resulting ocean-color-mean model and the observed range of ocean-color model estimates.

anomalous. However, the mean model provides a standard of consistency. If an anomalous model is closer to ‘truth’ (which can be evaluated in part 3 and in future ground-truth comparisons), its divergence from the mean model indicates that a majority of the models are far from truth.

In part 2 of the PPARR3 exercise, the sensitivity of the models to the input variables was examined by distributing data for 11 representative points, five from January 1998 and six from July 1998 (Table 2 and Fig. 2). These points correspond to a pixel (~18 km) and are chosen as representative of seasonal and geographic variability, as well as covering a range of input values and model response. We then systematically varied the value of each input variable, holding the others constant. The range of values for the input variables is roughly the range observed for our study period: for SST, -1 to 30 °C; for mixed-layer depth, 10–480 m; for PAR, 5 – 60 Ein $m^{-2} day^{-1}$; and for chlorophyll concentration, 0.01 – 10 mg m^{-3} . The final database consists of 385 values corresponding to the original data point and 34 variations at each geographical location. Carr and Friedrichs distributed these values to the participants who then estimated PP,

from which we estimated the difference in the decimal logarithm of PP for each perturbation of the input variable.

3. Results

3.1. Relationships among models

In PPARR2, production estimated from ocean-color algorithms was found to be highly correlated and the correlation was independent of model complexity (Campbell et al., 2002). In an attempt to group the models on the basis of related output, here we estimated pair-wise correlation and root-mean-square ($rms = \sqrt{\sum(\text{model}_i - \text{model}_j^2)/n}$) corresponding to the monthly global PP fields in January and July 1998 (Fig. 3). The correlation coefficient and rms between any pair of models is generally inversely related, with higher correlation between models with low rms (Figs. 3A and B). This is reassuring but not necessarily expected: correlation quantifies similarity in the variability while rms is a measure of mismatch. Perfectly coincident patterns may present a large systematic bias. The

Table 2

The points used for the sensitivity analysis

No.	Mon.	Lat.	Lon.	MLD	SST	PAR	CHL	PP	Range
1	Jul	−54.1	30.9	66.6	1.65	3.60	0.1758	0.0628	0.6697
2	Jan	16.2	66.1	71.8	26.40	42.	0.4955	0.9922	0.4366
3	Jan	33.8	−127.3	68.3	15.15	23.40	0.2951	0.4497	0.2876
4	Jan	−54.1	−162.4	32.5	6.90	41.10	0.5309	0.6914	0.3302
5	Jan	16.2	−39.4	70.3	24.75	38.40	0.1380	0.4543	0.39
6	Jul	−1.4	153.9	37.1	29.85	44.10	0.1012	0.3708	0.4279
7	Jul	−36.6	−39.4	63.0	16.05	15.60	0.2754	0.3570	0.3311
8	Jul	51.3	−21.8	15.7	15.	42.90	1.9724	1.8509	0.44
9	Jul	−1.4	−144.8436	22.9	24.45	51.	0.6095	1.1781	0.3828
10	Jul	33.8	153.9	10.7	25.05	49.50	0.1288	0.4769	0.4564
11	Jan	−36.6	83.7	15.7	18.75	52.50	0.2661	0.7507	0.4173

See Fig. 2 and text for details. No. denotes the numbering scheme (Fig. 2 and text); Mon. the month from which the data point was extracted; Lat. and Lon. are the latitude and longitude of the point; MLD is the mixed-layer depth at that location for that month in meters; SST is the sea-surface temperature in °C; PAR the photosynthetically available radiation in $\text{Ein m}^{-2} \text{day}^{-1}$; CHL is the chlorophyll concentration in mg m^{-3} ; PP is the depth-integrated primary production in $\text{g C m}^{-2} \text{day}^{-1}$; and Range is the observed range in ocean-color-based modeled PP in $\text{g C m}^{-2} \text{day}^{-1}$.

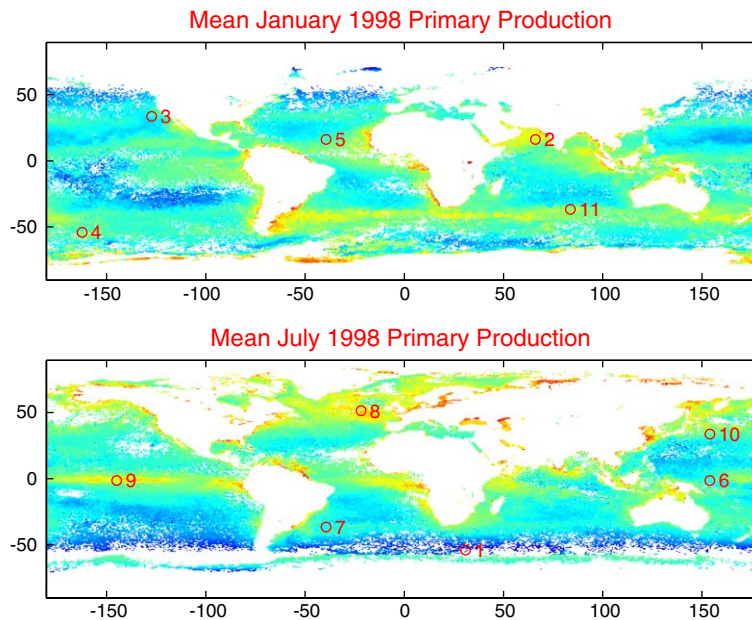


Fig. 2. Geographical location and point number, for points used in the sensitivity analysis (part 2 of PPARR3), overlaid on the mean model primary production for January and July 1998.

correlation among the ocean-color-based models is generally greater than 0.7 and always exceeds 0.5 (Fig. 3A). By contrast the GCM-based models are poorly correlated with the ocean-color models or among themselves ($r < 0.4$), with the exception of models #25/29 and #30/31 ($r > 0.66$). The rms values range between 0.2 and $0.4 \text{ g C m}^{-2} \text{day}^{-1}$ for the ocean-color models. The rms generally

exceed $0.4 \text{ g C m}^{-2} \text{day}^{-1}$ for the GCM-based models (Fig. 3B and D), except for #25/29 and #30/31 ($\text{rms} < 0.3$).

It is interesting to note that, as in the study of Campbell et al. (2002), neither model structure or type are the strongest predictor of relationship between model output. For example, model #24, a WRDR model, is most highly correlated to model

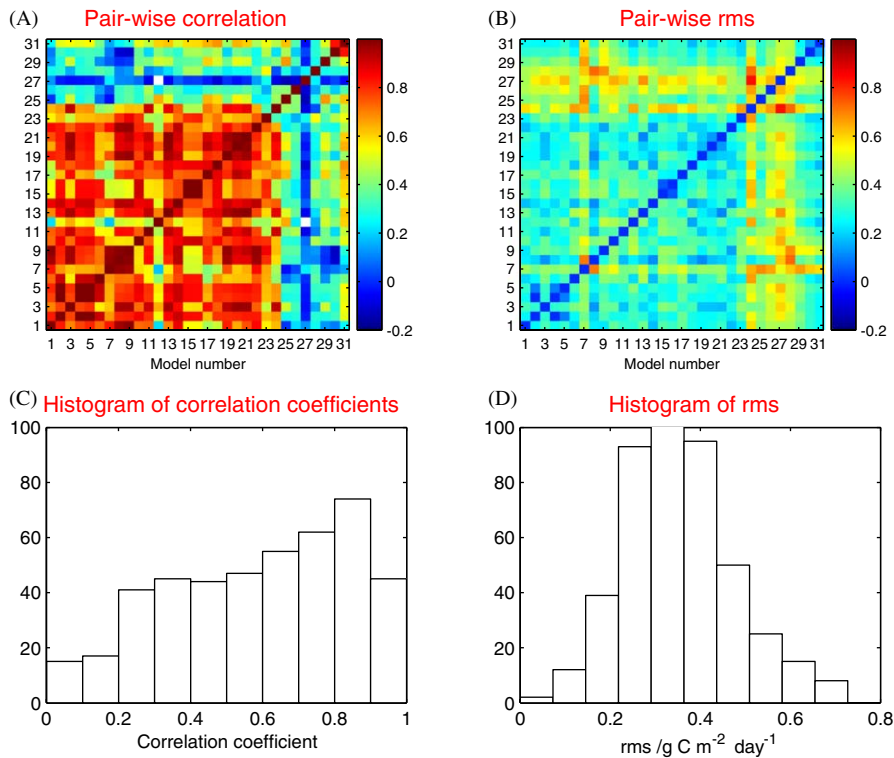


Fig. 3. Matrix of pair-wise correlation coefficients (A) and rms values (B) for the PP fields of January and July for each model. Histogram of correlation coefficients (C) and rms (D).

#3, a WIDI model, which only varies from #2 by the temperature dependence of the P_{max}^B . In turn, model #3 is more highly correlated with the WRDR models #20, 21, and 24 ($r > 0.92$) and with other WIDI models, than with model #2 ($r = 0.77$). Similarly, model #12, a variant of the Howard, Yoder, Ryan (HYR) model (Howard and Yoder, 1997), is correlated with models #18, 17, and 20 at $r > 0.7$, and is less correlated with the other HYR model variants.

A cluster analysis (Middleton, 2000) was carried out with the correlation matrix to group the models (Fig. 4). The correlation matrix is reduced to a single correlation coefficient via an iterative procedure: the two largest mutual correlations are identified; these two variables are merged together and the other variables take on an ‘average’ correlation within the reduced matrix (the unweighted pair-group method using arithmetic averages or UPGMA as in Rohlf, 1963). The results are expressed as a dendrogram. Five groups were distinguished.

Group 1 (Models #1, 8, 9, 14, 22, and 7): This group includes the simplest model, a WRDR model,

and four WIDIs: three variants of the vertically generalized production model (VGPM, Behrenfeld and Falkowski, 1997a) and a model based on neural networks. All the models in this group are highly correlated among themselves ($r > 0.82$). Four of the models in this group have no SST-dependence (#1, 8/9, and 22).

Group 2 (Models #10, 15, 16, 2, 4, 5, 6, and 23): This group has a WRDR model, the original VGPM, its twin (#4), and two additional VGPM variants (#5, 6), as well as two WIDR which parameterize P_{opt}^B following VGPM (#15, 16). All models in this group (except for #23) are correlated at $r > 0.8$. Group 2 is correlated to Group 1 with an $r \sim 0.65$.

Group 3 (Models #12, 18, and 17): This group includes two WIDR models and a WIDI (a HYR variant) which distinguishes integrated primary production within and below the mixed layer (#12). Model #12 does not use SST. These models are correlated at $r > 0.7$ and are more correlated to Group 4 than to the previous two groups.

Group 4 (Models #3, 13, 21, 20, 19, 11, 24): This group includes three WRDRs, a VGPM variant, an

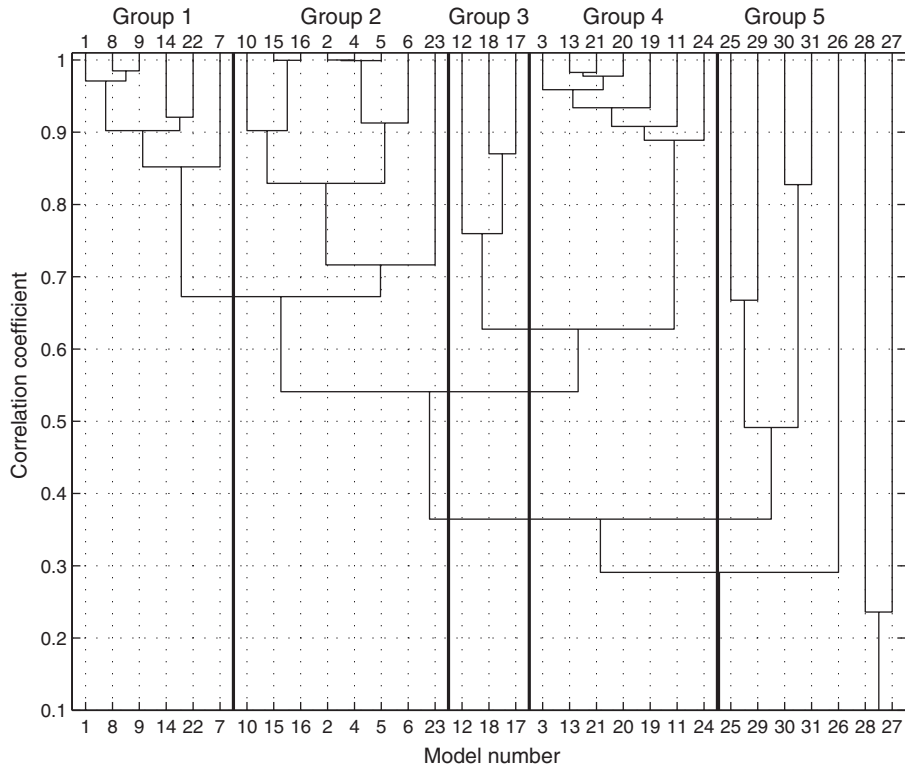


Fig. 4. Dendrogram of the models based on the matrix of pair-wise correlations for January and July.

absorption-based WIDR model, and two HYR variants. Five of these models use the Eppley (1972) parameterization of P_{\max}^B , and the WIDR (#19) uses an exponential function of SST to parameterize the attenuation coefficient for chlorophyll. These models are very highly correlated among themselves.

Group 5 (Models #25, 29, 30, 31, 26, 28, and 27): This group includes all of the GCM-based models, none of which cluster at $r = 0.7$. They are very weakly correlated among themselves as a group ($r < 0.4$) except for models #25 and 29 ($r > 0.65$) and #30 and 31 ($r > 0.8$), each pair of which are variants of the same model; the two pairs are correlated at $r \sim 0.4$. Model #26 is more correlated to Group 4 than to other models in the group, while #28 and 27 show little relationship with either the other GCMs or the ocean-color-based models.

Hereafter, the models are not portrayed in the graphs in their numerical numbering scheme, which follows complexity, but according to the relationship groups. The figures that break out the model estimates of PP according to basin, chlorophyll concentration, or SST level show that models with higher or lower than average PP are spread throughout the groups. However, group-related

trends are distinguished, likely resulting from similarities in parameterization.

3.2. Global PP

The mean global PP estimated from the ocean-color-based models for six months of 1998 (January, March, May, July, September, and November) is 50.7 Gt C y^{-1} (Fig. 5A). Average global values for the four ocean-color groups are 44, 55, 48, and 57 Gt C y^{-1} , respectively; the global mean PP is 55 Gt C y^{-1} for the GCM-based models. Global annual PP estimated by most of the GCM models is generally comparable to that of the ocean-color-based models. Model #28 represents a climatological year, which may explain some discrepancies.

The range of model estimates for the six-month average is 32 Gt C y^{-1} . Four ocean-color PP models fall at or below 40 Gt C y^{-1} , while five are at or above $\sim 60 \text{ Gt C y}^{-1}$. Most of the models, including GCMs, estimate PP within 49 and 60 Gt C y^{-1} . Group 1 PP estimates tend to be low, as are those of Group 3 (except for #17). By contrast, other than model #6, most models in Groups 2 and 4 are at, or above, the mean model. In terms of model structure,

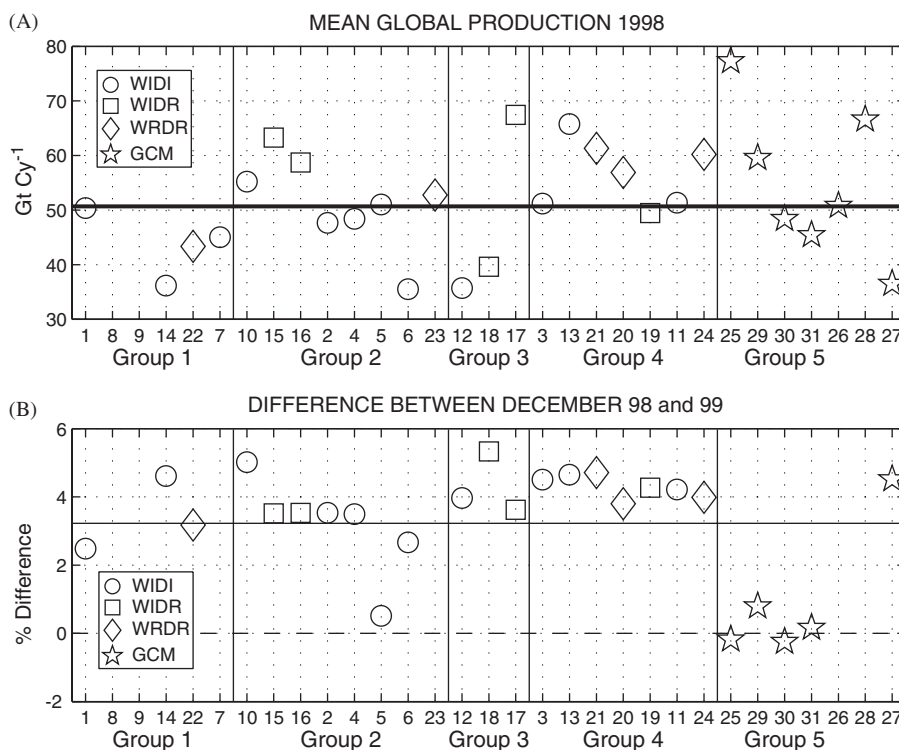


Fig. 5. The annual mean primary production for each model for 1998 (A) and a comparison between December of 1998 and December of 1999 (B). The models are ordered following the groups obtained from the cluster analysis and the five groups are separated by vertical lines. The horizontal line is the annual global production for the ocean-color-mean model (A) and the percent increase from December 1998 to December 1999 (B) for the ocean-color-mean model.

the VGPM variants are consistently close to the average model value with the exception of #6, which is low (Fig. 5A). The broadest range is observed among the WIDR models (#17 is very high while #18 is low) and the non-VGPM WIDI models (#13 is high, while #12 and 14 are low).

The observed range of values for global production (Fig. 5A) is comparable to that obtained from extrapolations of field measurements, such as those of Koblenz-Mishke et al. (1970) or Berger (1989), but it would be a mistake to interpret this as a lack of progress. Rather, the similarity lends credibility to our understanding of global marine photosynthesis. Ocean-color-based models allow us to document spatial and temporal variability on scales that are inaccessible to field programs.

We compared December 1998 with December 1999 to see if the models consistently captured variability between the two years (Fig. 5B). Global PP estimated by the ocean-color-based models is uniformly larger in December 1999 than in 1998 by on average 3%. Model #27 was the only GCM-based model that estimated a comparable difference

between the two Decembers to that of the ocean-color-based models (not surprising since forcing fields for interannual variability in the GCM-based models were different). The observed increase in PP likely results from the observed increase in both chlorophyll concentration and PAR in December of 1999 relative to December 1998.

3.3. Basin PP

We divided the world ocean into basins following Antoine et al. (1996) with the mask available at <http://marine.rutgers.edu/opp/Mask/MASK1.html>. The integrated PP in each basin is proportional to the basin areal extent in the Pacific, while the Atlantic and Indian tend to be slightly more productive and the Southern and Arctic Oceans tend to be less productive (Table 3). These differences are consistent with basin average latitude and the corresponding insolation. In all basins, the range between model estimates is as large as the mean; in the case of the Arctic Ocean, it is almost twice as large, reflecting both the small area and the

Table 3

Breakout of primary production estimated by ocean-color-based models for the ocean basins, chlorophyll concentration levels, and SST ranges

	Area, %	Mean/Gt C y ⁻¹ (%)	Min/Gt C y ⁻¹	Max/Gt C y ⁻¹	Range, %
<i>Basin</i>					
Pacific	45	21 (44)	15.5	30.9	72
Atlantic	23	12.8 (27)	9.1	17.9	68
Indian	17	9.9 (21)	6.9	15.1	83
Southern	13	2.6 (5.5)	1.1	4.9	149
Arctic	1.2	0.33 (0.7)	0.02	1.2	374
Med.	0.8	0.45 (0.95)	0.28	0.73	97
<i>Chl level</i>					
Oligotrophic	26–32	9.2 (19)	4.6	14.1	100
Mesotrophic	65–68	34.8 (70)	24.2	48.8	71
Eutrophic	3–5	5.6 (11)	2.4	9.9	136
<i>SST range</i>					
SST < 0 °C	2–4	0.52 (0.8)	0.17	2.1	372
0–10 °C	13–17	5.1 (10)	2.1	8.4	125
10–20 °C	~20	11.9 (25)	7.6	18.9	95
> 20 °C SST	~60	32 (64)	19.1	48.7	92

Area refers to percentage of global ocean area; mean is the average annual integrated primary production for 1998 (six months) for ocean-color model mean. The values in parenthesis (%) after the mean represent the percentage of the global mean integrated primary production. Min and max refer to the minimum and maximum model estimates and the range is the maximum minus the minimum expressed as a percentage of the mean model.

problems inherent to estimating primary production at high latitude (Table 3). The seasonal signal is best examined globally by looking at latitudinal bands (see Section 3.6); it is averaged out in the Atlantic and Pacific basins because the two hemispheres are out of phase. The pronounced seasonal signal in the Southern and Arctic Oceans reflects little or no production in hemispheric winter (Fig. 6). PP in the Pacific, Atlantic, and Indian basins is underestimated by Group 1 and overestimated by Group 4. Conversely Group 1 is high at high latitude, in the Southern and Arctic Oceans. The PP estimate of the GCM-based models of Group 5 is higher than the ocean-color models in the Pacific and Southern Ocean, but is comparable to them in the Atlantic, Indian, and Arctic basins (Fig. 6).

The deviation between each model/monthly value and that of the mean model is shown in Fig. 7. The deviation is expressed as the difference between the decimal logarithm of that model/month and that of the ‘mean’ model for that month. The ratio of the model mean and the multi-model mean is written within the box when the difference of the logarithms exceeded ± 0.32 , i.e. when the model was smaller or larger by an approximate factor of two than the mean. We consider the models that diverge beyond

this criterion for more than one month to be anomalous.

No ocean-color-based model is anomalous in the Atlantic, Pacific, or Indian Oceans, and only two are anomalous in the Mediterranean (Fig. 7). There are six anomalous models each in the Southern Ocean and Arctic (Fig. 7). In the Southern Ocean, models #1 and 10 counter the seasonal cycle by estimating lower PP in austral summer. Four models reinforce the seasonal cycle with decreased austral winter values (models #8 and 18) or by enhanced PP in austral summer (#7 and 23). Model #12 is anomalously low through the year. All GCM-based models estimate significantly higher Southern Ocean PP for austral winter (#25, 29, 26) or all of the year (#28 and 27). Southern Ocean PP in model #31 is very close to that of the mean model. The Arctic presents the most extreme anomalous results for the ocean-color-based models: the PP is very small in models #12, 11, and 24, while models #1, 7, and 19 estimate higher PP than the mean. The GCM-based models are comparable to the ocean-color mean except for higher PP in the boreal winter. Summer PP estimated by models #11 and 24 is anomalously low in the Mediterranean, while #12 and 18 are anomalously low in boreal winter.

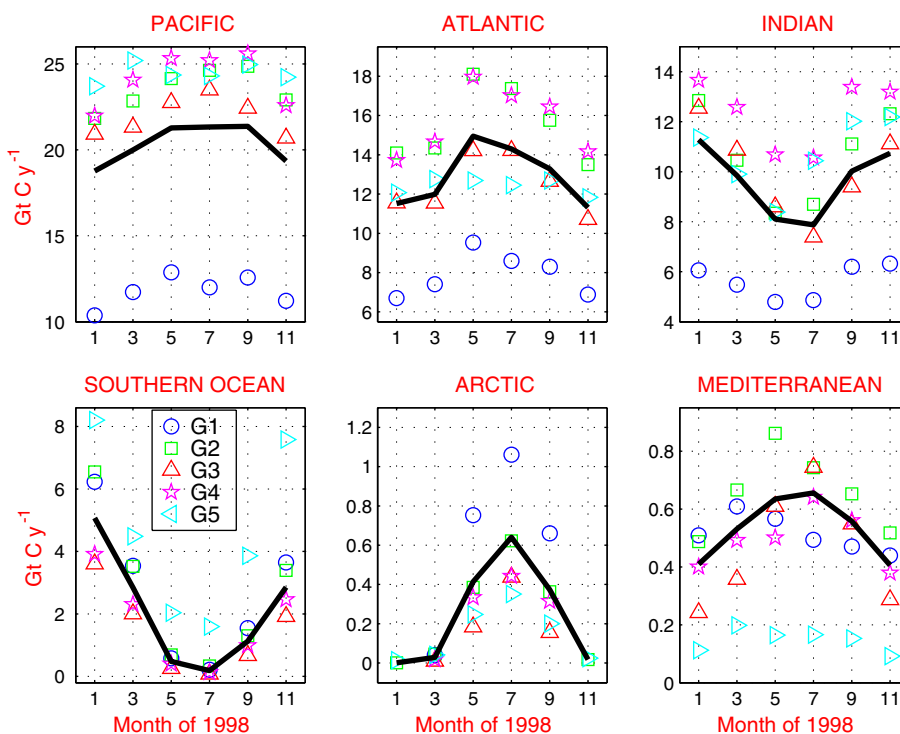


Fig. 6. The monthly progression of the PP (expressed as an annual value) within each basin for the ocean-color-mean model (thick line) and the monthly average of each of the five groups, denoted here as G1 through G5. Note that the range of area-averaged PP changes in each basin/panel.

GCM-based models #26, 30 and 31 have no Mediterranean basin, and the other models of Group 5 generally underestimate PP in this basin, especially in winter months.

3.4. Chlorophyll concentration levels

We divided the global fields into levels of chlorophyll concentration, i.e. oligotrophic ($<0.1 \text{ mg Chl m}^{-3}$), mesotrophic ($0.1\text{--}1 \text{ mg Chl m}^{-3}$), and eutrophic waters ($>1 \text{ mg Chl m}^{-3}$), to evaluate the model performance for these conditions (Fig. 8). Although, there is a variable apportioning in each category from month to month, concentrations are consistently less than 1 mg Chl m^{-3} for $\sim 95\%$ of the ocean (Table 3). As expected from the area, the bulk of global PP occurs in mesotrophic waters, $\sim 35 \text{ Gt Cy}^{-1}$, or 70% (Fig. 8 and Table 3). Integrated PP in eutrophic waters is about half that of oligotrophic ones, although their area is 6–10 times smaller (Fig. 8 and Table 3). The normalized range between models varies most for eutrophic waters (Table 3 and Fig. 8). Systematic differences between the groups can be distinguished among the

chlorophyll concentration levels. PP estimated by Group 1 is much lower than the mean in oligotrophic and mesotrophic regions, while that of Group 3 is lower than the mean model for eutrophic waters, but is higher than the mean in oligotrophic waters. Since the majority of global PP occurs in mesotrophic regions, this explains why Group 1 estimates lower global PP than the mean model (Figs. 5 and 8). Groups 2 and 4 have higher PP in mesotrophic, and Group 4 is much higher under eutrophic conditions.

It should be noted that the GCM-based models do not use ocean color, so the eutrophic areas for models #1 through 24 are unlikely to coincide with models 25 through 29. We compared the chlorophyll fields for models #25 and 29 with the input fields used here. The area in which chlorophyll concentrations are eutrophic is 30% (#29) to 60% (#25) smaller than in the SeaWiFS fields. The oligotrophic and mesotrophic areas are within 10% for #25 though the oligotrophic area is 50% larger in #29. PP from Group 5 is higher than the ocean-color mean when chlorophyll is less than $0.1 \text{ mg Chl m}^{-3}$, while it is much lower in eutrophic

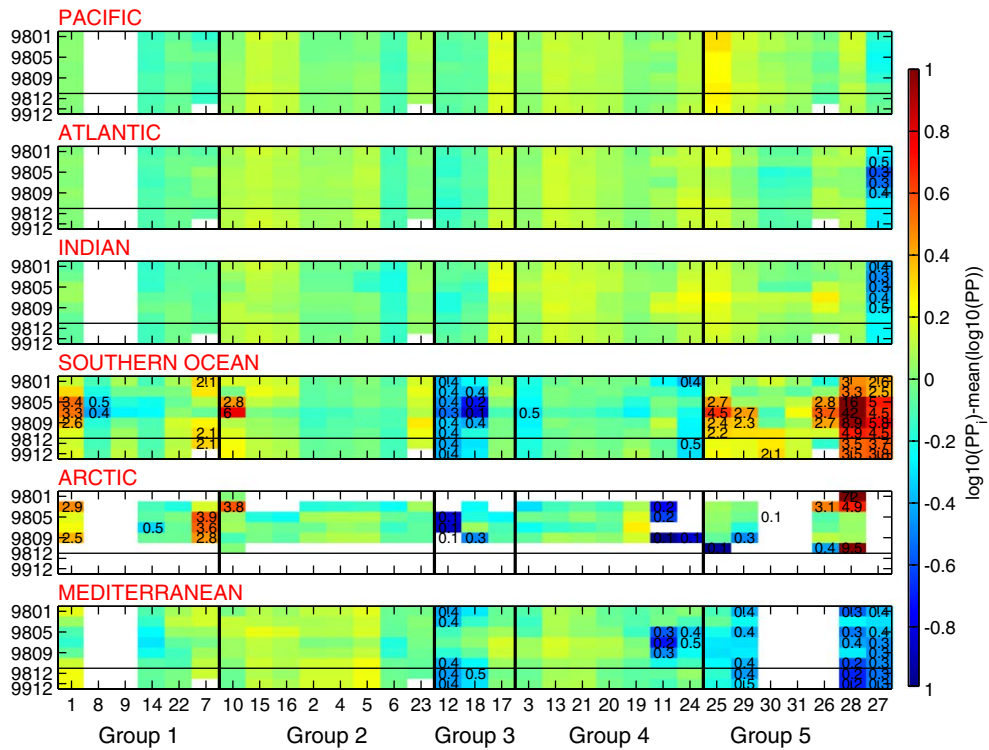


Fig. 7. Comparison between monthly PP of each model within each basin and that of the ocean-color-mean model. Models are ordered following the dendrogram and the five groups are separated by vertical lines. The horizontal line separates the six months of 1998 from December 1998 and 1999. When the comparison exceeds a factor of two, the ratio is written within the box. A white box denotes missing data or very small numbers.

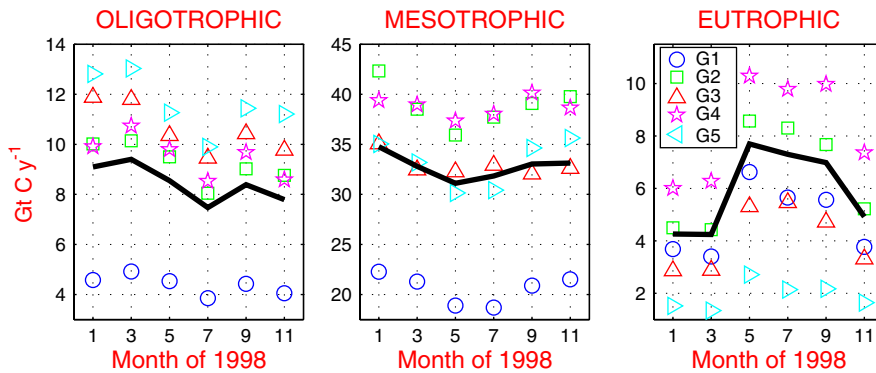


Fig. 8. The monthly progression of the PP (expressed as an annual value) within each chlorophyll level for the ocean-color-mean model (thick line) and the monthly average of each of the five groups, denoted here as G1 through G5. The chlorophyll levels are oligotrophic ($<0.1 \text{ mg Chl m}^{-3}$), mesotrophic ($0.1\text{--}1 \text{ mg Chl m}^{-3}$), and eutrophic ($>1 \text{ mg Chl m}^{-3}$). Note that the range of area-averaged PP changes in each chlorophyll level/panel.

regions. This is consistent with the GCMs having fewer very high values.

Model output diverges most for low and high chlorophyll concentration levels, but there is only one anomalous ocean-color model in eutrophic

waters (#12, Fig. 9). Although the differences are less than a factor of two from the mean model, there are distinct tendencies in some models and groups. For example, model #6 is low for mesotrophic and eutrophic waters but close to the mean for

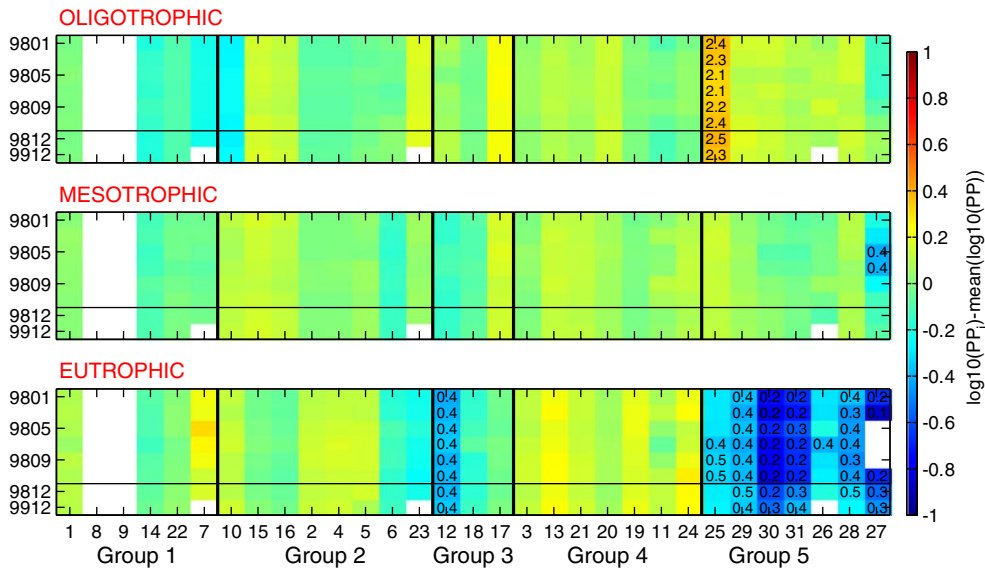


Fig. 9. Comparison between monthly PP of each model within each chlorophyll level and that of the ocean color mean model. Models are ordered following the dendrogram and the five groups are separated by vertical lines. The horizontal line separates the six months of 1998 from December 1998 to 1999. When the comparison exceeds a factor of two, the ratio is written within the box. A white box denotes missing data or very small numbers.

chlorophyll less than $0.1 \text{ mg Chl m}^{-3}$, while models #23, 15, and 16 are low for eutrophic, and high for oligo- and mesotrophic waters (Fig. 9). Models #7 and 13 are anomalously high for eutrophic waters and normal to low for oligotrophic waters. All GCM-based models are anomalously lower than the model mean in eutrophic waters and overestimate PP in oligotrophic conditions.

3.5. SST bins

SST is used to parameterize maximum photosynthetic rates in many ocean-color-based models, so we divided our data-set into SST bins: T1, below 0°C ; T2, from 0 to 10°C ; T3 from 10 to 20°C ; and T4, exceeding 20°C . As in the chlorophyll concentration levels, the percent area in each SST bin varies seasonally; in approximate terms SST exceeds 20°C in 60% of the global ocean, while it is below 0°C in 2–4%. In many PP models, maximum photosynthetic rate increases with SST, so the corresponding contribution of SST bins greater than 10°C to global PP is about 5% higher than their corresponding area: ~ 12 and 32 Gt C y^{-1} for T3 and T4, respectively (Table 3). Group 1, which includes models with no explicit SST-dependence, underestimates PP compared to the mean when SST exceeds 10°C (T3 and T4) and tends to over-

estimate mean PP for very low SST (Fig. 10). The PP estimated by Group 2, which includes several VGPM variants which estimate maximum P_{opt}^B at intermediate SST, is much higher than the mean for SST between 0 and 20°C (T2 and T3) and is lower for T4. Models in Group 4, which use an exponentially increasing function of SST to parameterize P_{max}^B or the attenuation coefficient for light, estimate significantly higher PP in T4 than the mean model. Modeled production varies by a factor of 3 for SST less than 10°C (Table 3 and Fig. 10). Although the divergence of models at low temperatures has relatively low impact globally, it is very significant at high latitudes, such as the Southern Ocean.

As expected, there are several anomalous models below 0°C : models #1 and 7 from Group 1 and #10 from Group 2 are consistently higher than the multi-model mean while models #5, 6, 12, and 24 are consistently low (Fig. 11). Only models #12 and 18 of Group 3 are anomalously low for T2 although models in Group 1 generally overestimate PP with respect to the mean. PP below 10°C estimated by GCM-based models #27 and 28 is higher than the multi-model mean; although SST is also likely to be different for the GCM model runs, the systematic bias for low SST is likely significant. For SST values exceeding 10°C , there are no anomalous

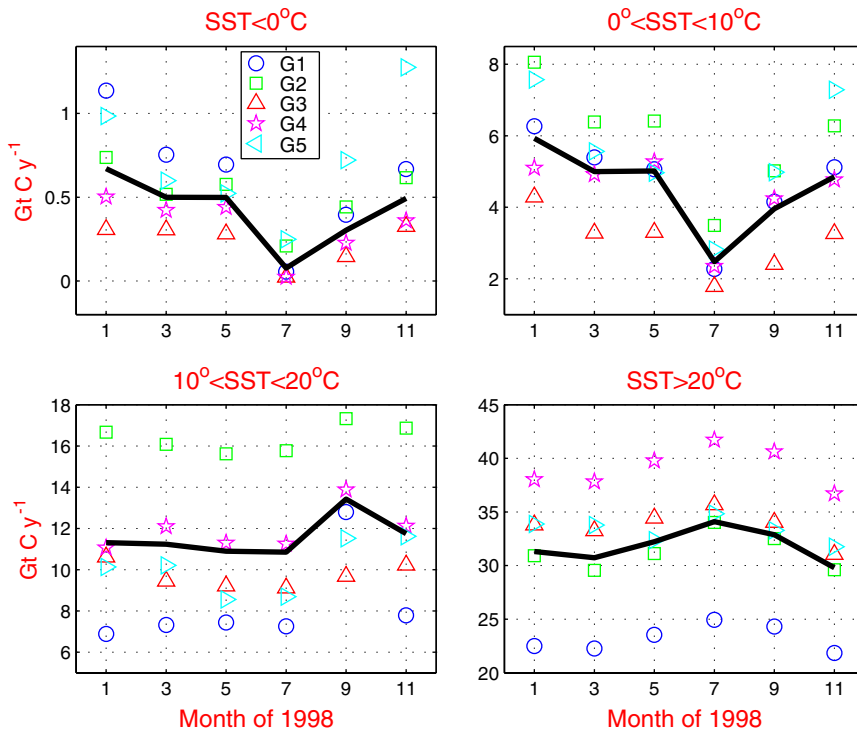


Fig. 10. The monthly progression of the PP (expressed as an annual value) within each SST bin for the ocean-color-mean model (thick line) and the monthly average of each of the five groups, denoted here as G1 through G5. Note that the range of area-averaged PP changes in each SST bin/panel.

ocean-color models. However, most models in Group 2 overestimate PP in T3, while Groups 1 and 3 underestimate relative to the mean for $SST > 20^\circ\text{C}$. PP below 0°C and for SST exceeding 20°C is higher in 9912 than in 9812, likely because of interannual variability in global temperatures (not shown).

3.6. Seasonal differences in latitudinal bands

The primary production of the mean model averaged within latitudinal bands is consistent between basins, with the exception of the highly productive northern Indian Ocean (Fig. 12). Maximum PP occurs in the equatorial band (10°S – 10°N) of all three basins ($>0.5\text{ g C m}^{-2}\text{ day}^{-1}$) and between 10 and 40°N in the Indian Ocean ($\sim 0.75\text{ g C m}^{-2}\text{ day}^{-1}$). Minimum PP values occur poleward of 40° in hemispheric winter where they are comparable to those of the remainder of the basin in hemispheric summer ($\sim 0.35\text{ g C m}^{-2}\text{ day}^{-1}$). Average PP between 10 and 40°S is lower than the corresponding band in the northern hemisphere. The seasonal cycle is very pronounced

poleward of 40° and it decreases moving equatorward except in the northern Indian Ocean. The Pacific equatorial band shows a maximum later in the year, which may reflect interannual variability associated with the 1997–1998 El Niño rather than a seasonal progression.

Fig. 13 shows how the models diverge from the mean model in global latitudinal bands. The features were essentially the same for individual basins, except for model #6 which has anomalously low PP in the northern Indian Ocean (not shown). Model #1 is consistently higher than the mean in hemispheric winter poleward of 40° , while models #12 and 18 are consistently low. Model #7 is generally high in summer north of 40°N . Several models in Group 2 (#10, 14, 15, 2, 4, and 5) tend to overestimate PP relative to the mean poleward of 40° , but not anomalously so. By contrast this group underestimates PP in the equatorial region of all three basins, in the case of model #6 by over a factor of two. Model #17 of Group 3 and #24 of Group 4 are generally high in the tropics and subtropics. All the models of Group 4 overestimate PP in the equatorial band and underestimate it poleward of

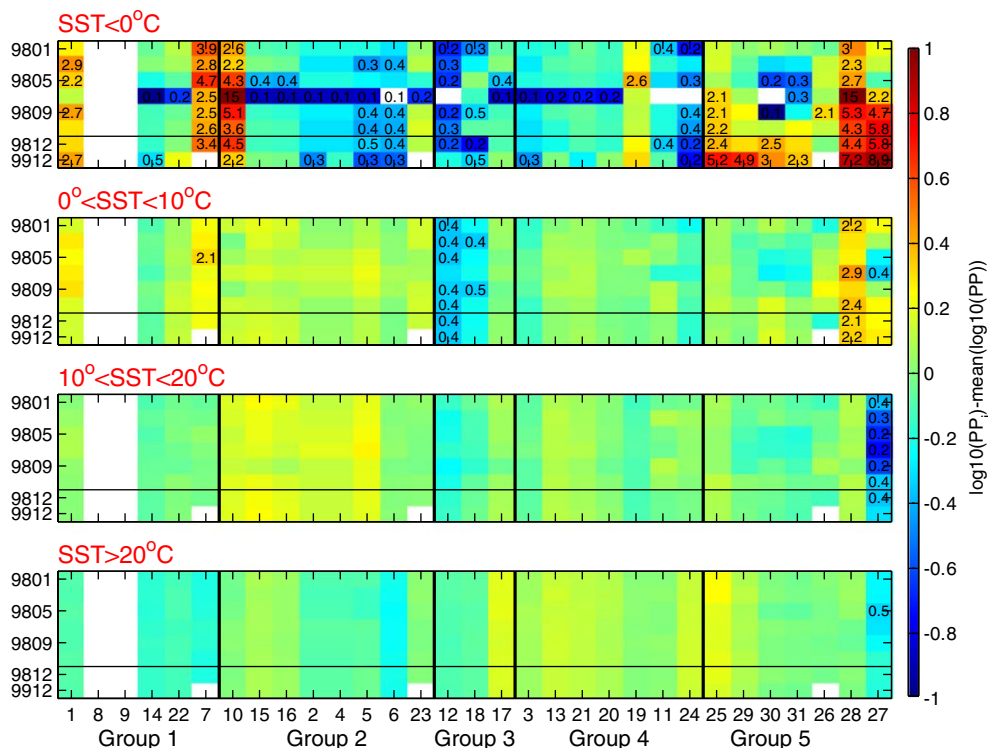


Fig. 11. Comparison between monthly PP of each model within each SST bin and that of the ocean-color-mean model. Models are ordered following the dendrogram and the five groups are separated by vertical lines. The horizontal line separates the six months of 1998 from December 1998 and 1999. When the comparison exceeds a factor of two, the ratio is written within the box. A white box denotes missing data or very small numbers.

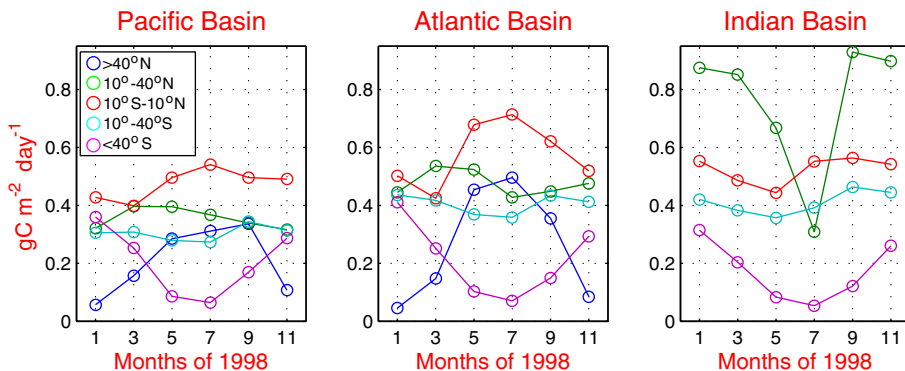


Fig. 12. Monthly progression of area-integrated PP (expressed as an annual value) of the ocean-color-mean model within latitudinal bands in each basin.

40°. The GCM-based models, especially model #27, tend to overestimate ocean-color mean PP in the equatorial region. Models #27 and 28 obtain higher PP than does the mean ocean-color model poleward of 40°S, while #30 and 31 underestimate PP poleward of 40°N.

3.7. Sensitivity analysis

This analysis examines the effect of the input variables on the ocean-color-based determination of primary production. The GCM-based models did not carry out this exercise as they do not use the

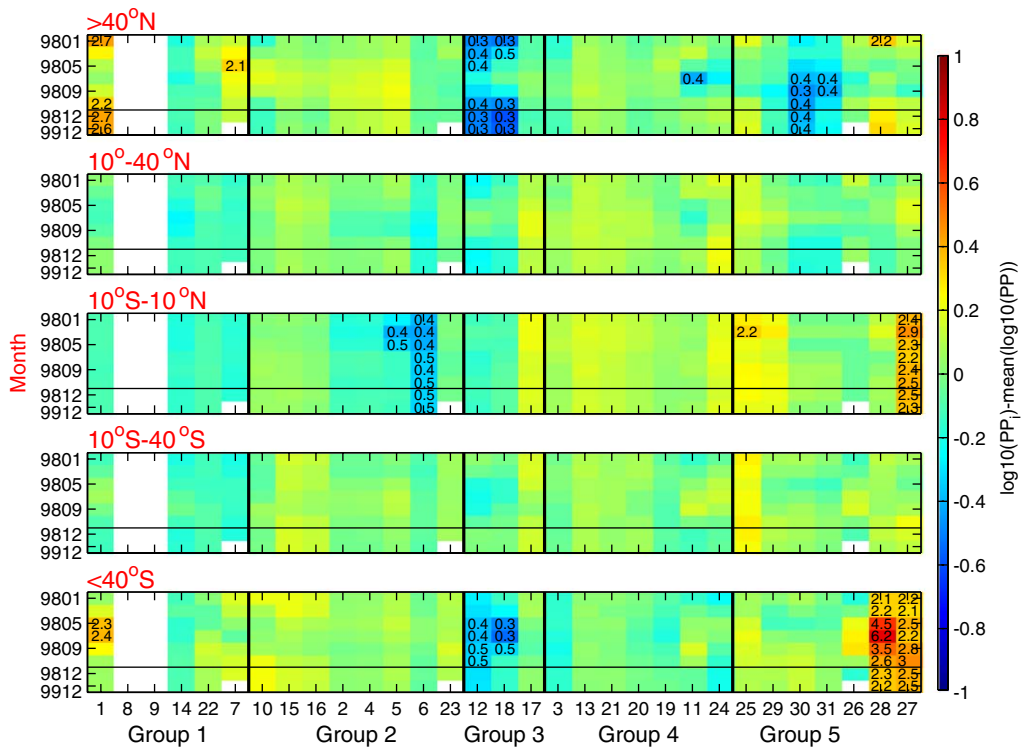


Fig. 13. Comparison between monthly PP of each model within latitudinal bands and that of the ocean-color-mean model. Models are ordered following the dendrogram and the five groups are separated by vertical lines. The horizontal line separates the six months of 1998 from December 1998 and 1999. When the comparison exceeds a factor of two, the ratio is written within the box. A white box denotes missing data or very small numbers.

input fields nor is it trivial to change the forcing values at specific locations. Starting with the 11 'representative' points of Table 2 and Fig. 2, we systematically varied the mixed-layer depth, SST, PAR, and chlorophyll concentration within a range of reasonable values, holding the other input variables at their original magnitude. We then plot the impact in simulated primary production (ΔPP) at each location corresponding to the change in each of the four input variables for each model, (ΔMLD , ΔSST , ΔPAR , and ΔChl). Because the variation in the input variables is unrealistic for some locations, we have reduced the axes of the plots to correspond to the observed range of input variables at the study points. We only show the most extreme and characteristic points in these plots (points 1, 2, 4, 7, 8, 10, and 11) that are evenly distributed between January and July (Table 2). A subset of ocean-color-based models have contributed to part 2 (Table 1).

Only six models use mixed-layer depth (Fig. 14; models #14 of Group 1, #23 of Group 2, #12 of

Group 3, and #20, 11, and 24 of Group 4). The impact of changing mixed-layer depth is less than a factor of two except for model #11 (which integrates to mixed-layer depth instead of to euphotic depth) where PP almost triples in response to increased mixed-layer depth. In two models (#11 and 14) deepening mixed layers increases PP asymptotically. Models #20 and #23 are insensitive to ΔMLD . Model #12 shows maximum impact for changes of order 50 m, which primarily lead to decreases in PP. Model #24 presents peak ΔPP at ΔMLD of 75–100 m, which then decreases for deeper mixed layers. In model #20, ΔPP is weakly negative for positive ΔMLD , while model #23 responds primarily, if weakly, to negative ΔMLD . Points 10, 11, and 8 are most sensitive; these points have shallow initial mixed-layer depths (Fig. 2 and Table 2).

All models except for #1, 8/9, and 22 (in Group 1) and #12 (Group 3) use SST (Fig. 15). There seem to be four responses to SST perturbations, which can be seen best for the full range of perturbation (Fig. 16): a gaussian shape (#2/4, 5, 6), a linear

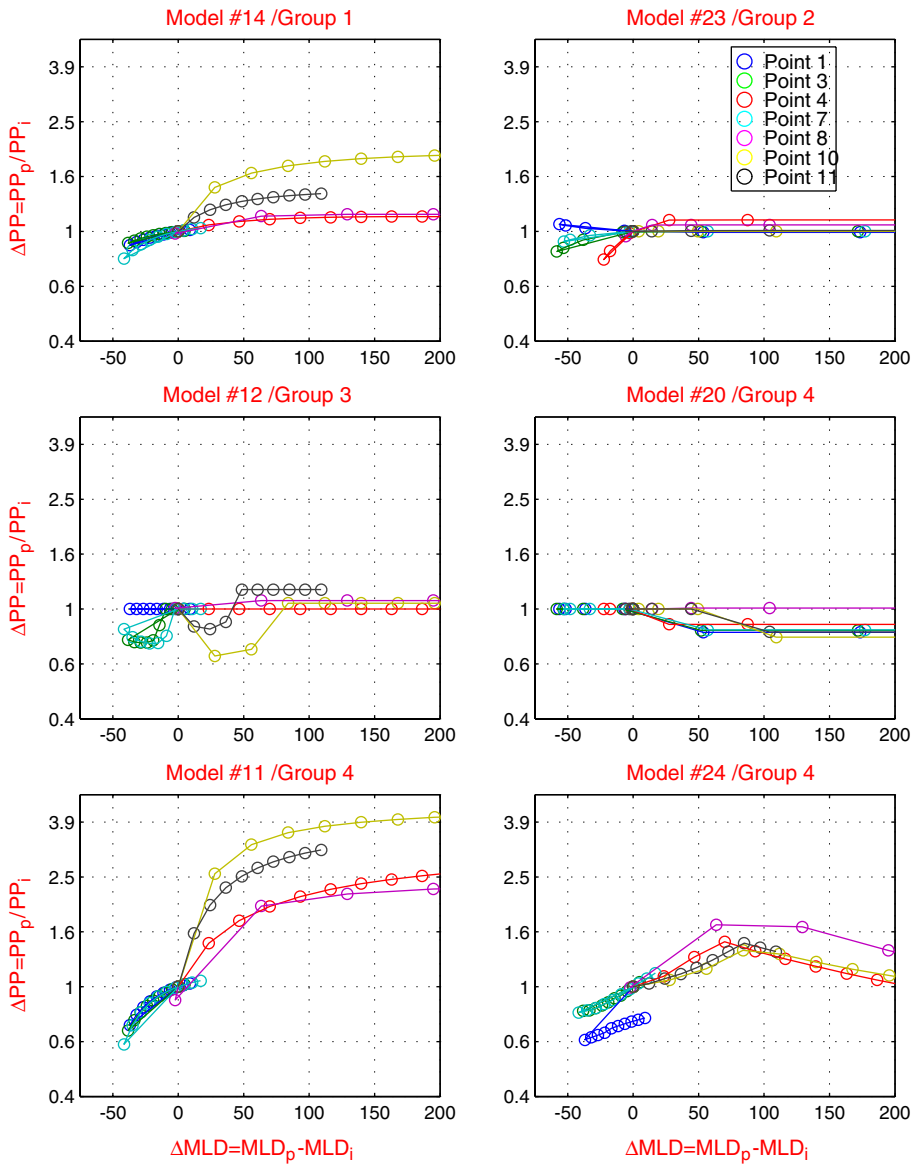


Fig. 14. Sensitivity of the ocean-color models to perturbations in mixed-layer depth. The subscripts p and i refer to the perturbation and the initial values, respectively. We focus on a subset of points from Table 2, and on the observed range of variability at those points. The ocean-color models that participated in part 2 (Table 1) that are not depicted here show no response to perturbations in mixed-layer depth. Model #8/9 only did the sensitivity study for the two Southern Ocean points.

increase (#3, 20, 21, and 24), an asymptotic-linear form (#11, 13, 17, 18, and 23), and finally, in model #19, ΔPP increases weakly for decreasing negative ΔSST to an inflection point (not always $0^\circ C$) after which it increases more sharply. The Gaussian shape results from the polynomial function of SST used in the VGPM and some of its variants; maximum ΔPP occurs at $SST \sim 20^\circ C$ for Model #2/4, or 5 and at $\sim 15^\circ C$ for Model #6 (Fig. 16).

The models that have a linear or asymptotic response consistently have negative ΔPP for negative ΔSST . By contrast, the models with a central maximum present peak ΔPP at both positive and negative ΔSST for different points (Fig. 16). A key difference between model responses seems to be whether ΔPP increases with positive ΔSST (Group 4). The points that were most sensitive to positive ΔSST are points with low initial SST

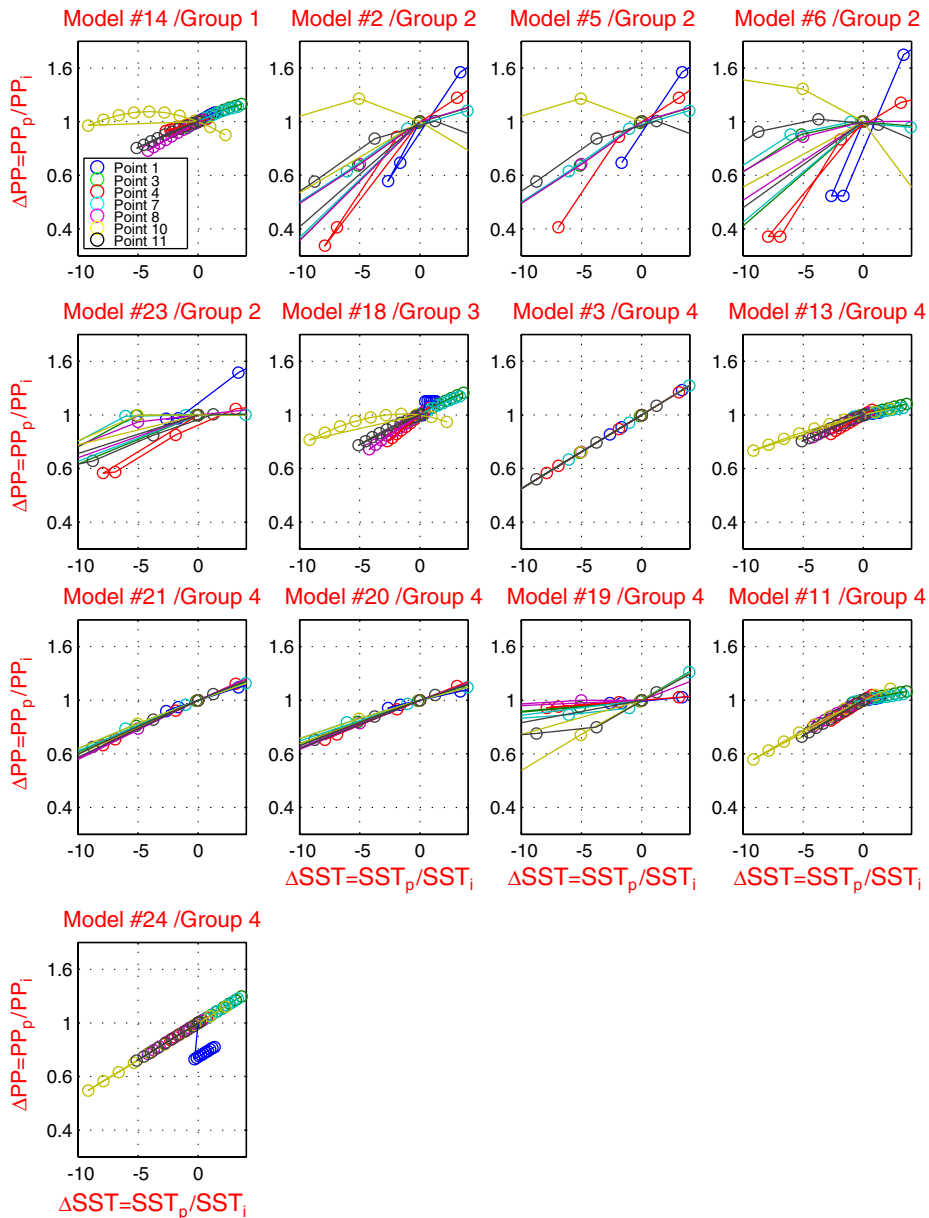


Fig. 15. Sensitivity of the ocean-color models to perturbations in SST. The subscripts p and i refer to the perturbation and the initial values, respectively. We focus on a subset of points from Table 2, and on the observed range of variability at those points. The ocean-color models that participated in part 2 (Table 1) that are not depicted here show no response to perturbations in SST. Model #8/9 only did the sensitivity study for the two Southern Ocean points.

(1 and 4), while points with warm SST and shallow mixed-layer depths (11 and 10, see Table 2) were more sensitive to negative ΔSST .

All models, except for #1, increase their PP asymptotically in response to positive ΔPAR (Fig. 17). For ‘average’ initial PAR values, perturbations lead to a quasi-linear response following a slope that is

either shallow (model #14) or sharp (model #18). ΔPAR exceeding $30 \text{ Ein m}^{-2} \text{ day}^{-1}$ impacts PP by a factor of 10 in models #12, 18, 13, and 11 for point 8 (northeast Atlantic with high original PAR) and for point 1 (a Southern Ocean location with very low original PAR) (Figs. 2 and 19, Table 2). The VGPM variants are generally insensitive to changes in PAR

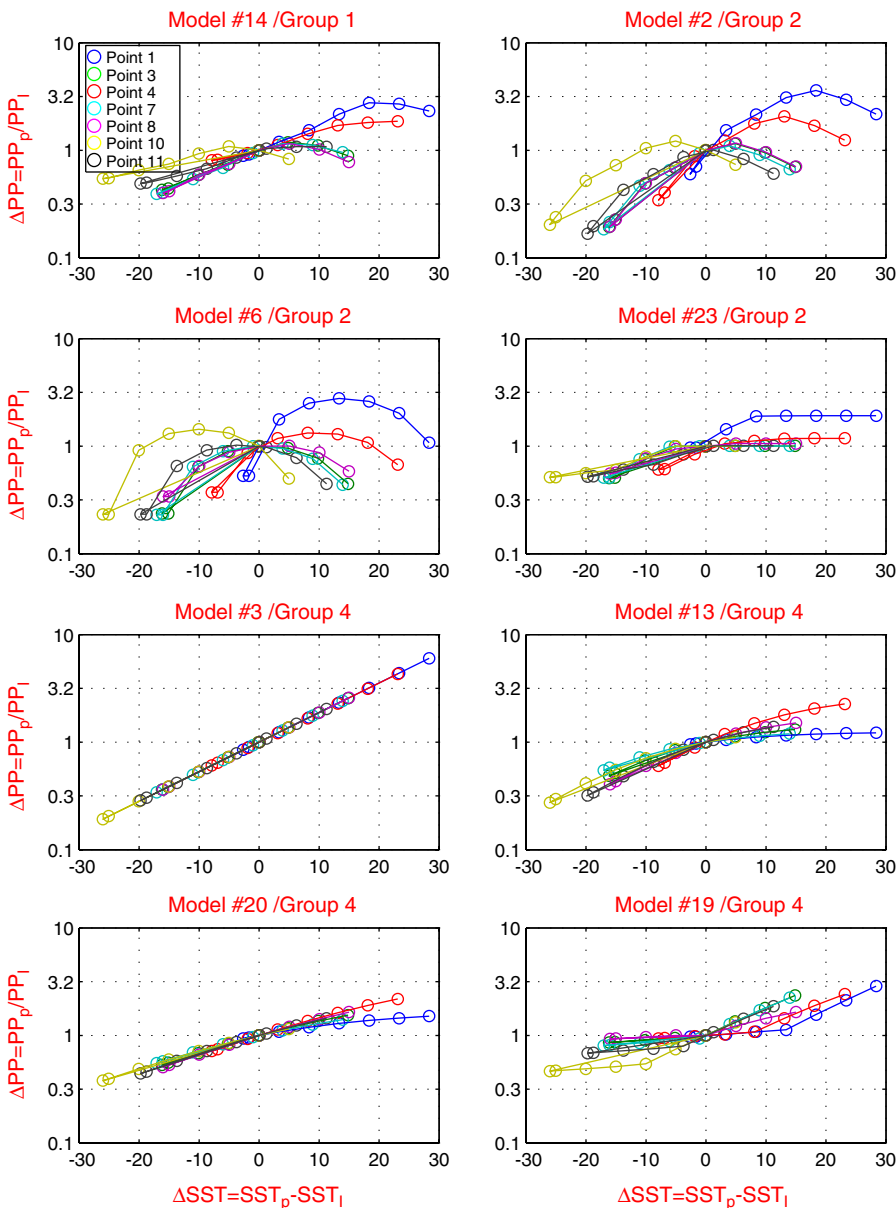


Fig. 16. Sensitivity of a subset of ocean-color models to the full range of perturbations in SST. The subscripts p and i refer to the perturbation and the initial values, respectively. The response of models #4 and #5 (not shown here) is identical to that of #2.

(ΔPP much less than a factor of two), except for point 1. The most sensitive models are the HYR variants (#11, 12, 13) and the WIDR #18.

By far the most important input variable is chlorophyll concentration (Fig. 18). All models present a positive quasi-linear relationship for logarithmic-scale changes. Changing chlorophyll concentration by a factor of four translates to a

change in PP of about a factor of three in all models. Higher response is seen in models #11 and 21 of Group 4, while model #23 is less sensitive. In most models the response is comparable for different points. However, models #6 (Group 2), 19 and 21 (both of Group 4) show a spread of responses, with greatest ΔPP for the points with lowest original chlorophyll (e.g., points 1 and 10).

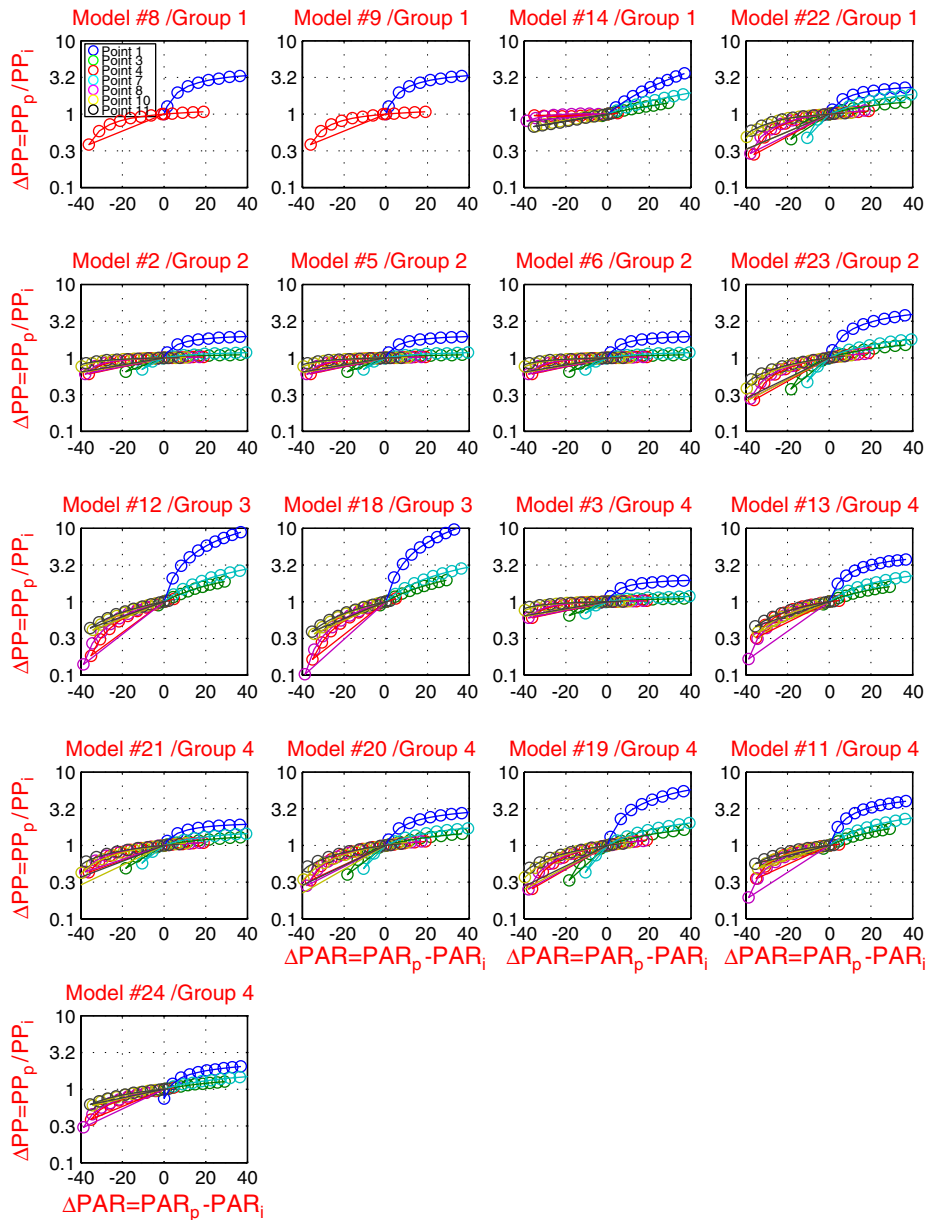


Fig. 17. Sensitivity of the ocean-color models to perturbations in PAR. The subscripts p and i refer to the perturbation and the initial values, respectively. We focus on a subset of points from Table 2, and on the observed range of variability at those points. The ocean-color models that participated in part 2 (Table 1) that are not depicted here show no response to perturbations in PAR.

Models #6 and 19 use chlorophyll concentration to determine the maximum photosynthetic rate, leading to more complex dependencies (Fig. 18).

The sensitivity analysis is by no means a measure of error. Marine photosynthesis depends on the input variables, either directly or indirectly. All of the ocean-color-based PP models discussed here are driven by chlorophyll concentration and, except for

model #1, PAR. Most models also use SST or mixed-layer depth to quantify maximum photosynthetic rate and/or to characterize the environmental conditions experienced by the cells. The range of sensitivity for the different models impacts their divergence under different environmental conditions as well as their ability to reflect temporal variability, such as heating or increased stratification on a range

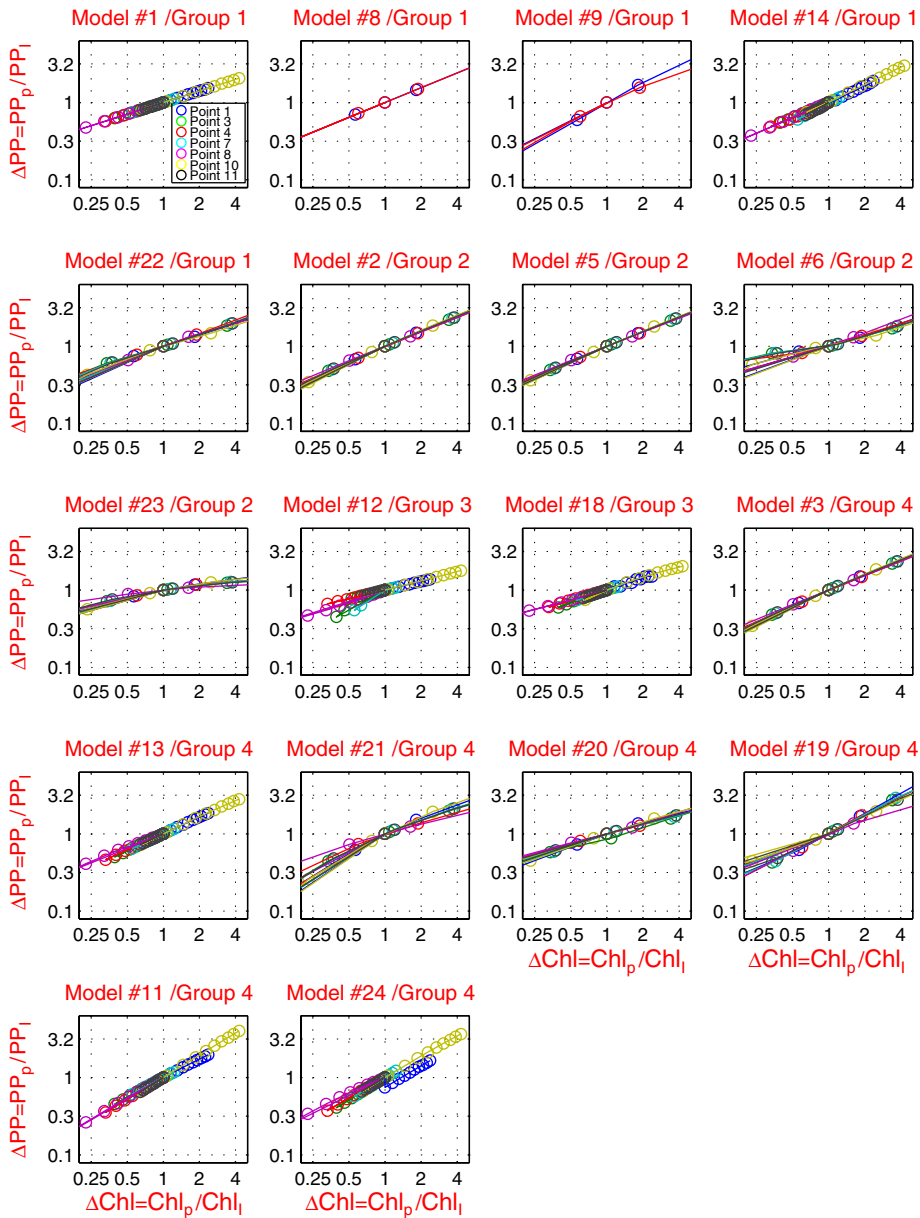


Fig. 18. Sensitivity of the ocean-color models to perturbations in chlorophyll concentration. The subscripts p and i refer to the perturbation and the initial values, respectively. We focus on a subset of points from Table 2, and on the observed range of variability at those points. All ocean-color models that participated in part 2 (Table 1) responded to perturbations in chlorophyll concentration. Model #8/9 only did the sensitivity study for the two Southern Ocean points.

of temporal or spatial scales. The simplest PP model (#1), which depends only on chlorophyll concentration, led to a reasonable global estimate (Fig. 5A) but excessively high values at low PAR or SST (Figs. 7, 11, and 13 and Table 4). The dependence on SST, especially with regards to the formulation of the maximum photosynthetic rate, seems to impact the groups, regardless of model complexity. Some of

the groups cannot be completely evaluated as we are missing contributions from some model participants.

3.8. Correlation between PP and input variables

The pair-wise correlation between primary production and the input variables (SST, mixed-layer depth, PAR, and chlorophyll concentration) for

Table 4
Outlier models compared to the ocean-color-mean model

	P	A	I	S	T1	T2	T3	T4	O	M	E	PN	STN	EQ	STS	PS
#1				H ^a	H	h ^a						H ^b				H ^a
#8				L ^a												
#7				H ^b	H	h					h ^a					
#10				H ^a	H				l			h ^a				h ^a
#15					L ^a						l					
#16					L ^a						l					
#5					L							h ^a		L		
#6					L									L		
#23				H ^b												
#12				L	L	L					L	L ^b				L ^a
#18				L ^a	L	L					l	L ^b				L ^a
#17								h	h		l			h		
#13												h				
#24				L ^b	L							h ^b				
#25				H ^a	H			h	H		L ^b	L		h	h	
#29											L	L				
#30				H ^a							L	L				
#31											L	L ^b				
#26				H ^a												
#28				H	H	H					L					H
#27		L	L	H	H		L	l		L ^a	L			H		H

The columns A, P, I, and S refer to the Atlantic, Pacific, Indian and Southern Oceans. T1 through T4 correspond to the SST bins, O, M, and E to oligotrophic, mesotrophic and eutrophic chlorophyll levels. PN and PS correspond to poleward of 40°, north and south, respectively; STN and STS refer to the subtropical regions (10–40°) north and south, respectively, and EQ to the equatorial region. Within the table L refers to a low value and H to a high value compared to the multi-model mean. When l or h are in lower case the model was larger or smaller than the mean model, but by less than a factor of two.

^aindicates an anomaly from only May–September and

^bindicates anomalies in boreal winter.

January and July 1998 indicates that the relationship between forcing and PP response is consistent within groups (Fig. 19). In all ocean-color-based models PP is positively correlated with chlorophyll (on average $r = 0.65$), but correlation is generally weak or weakly negative with PAR and SST, except for a few models. Beyond this, the correlations vary between the different groups.

The highest correlation between chlorophyll and PP is seen in Groups 1 and 4 ($r = 0.87$ and 0.8 , respectively), while in Group 2 and 3 they are correlated at ~ 0.6 . The GCM-based models in Group 5 show essentially no relationship between PP and the ocean-color chlorophyll concentration, except for models #31 and 26 at $r \sim 0.4$. PP estimated by Group 3 and by models #15, 16, and 23 (the models of Group 2 that are not VGPM variants) is positively correlated with PAR ($r \sim 0.6$); in these models PAR explains more or an equal amount of

the PP variance as chlorophyll concentration. Models #13, 21, and 20 (Group 4) are weakly correlated with PAR as well ($r \sim 0.5$). SST has a weak negative correlation with the PP estimated by the models in Group 1 (although SST is not used by four of the models), as well as in the VGPM and several of its variants (Group 2). Conversely it is more highly correlated ($r \sim 0.5$) when the correlation with PAR exceeds 0.6 in both Groups 2 and 3. PP is uniformly weakly correlated with SST at $r \sim 0.2$ for Group 4. By contrast, PP from models #10, 14, and 15 (Group 2) and #12 (which does not use SST) and 18 (Group 3) is positively correlated with SST at $r \sim 0.5$. In the remainder of the models SST shows a weak positive correlation with PP. Mixed-layer depth is negatively correlated to PP at ($r \sim -0.2$ to -0.4) or uncorrelated, including the models that integrate PP to the depth of the mixed layer (#10, 11, and 12). Not surprisingly, the intensity of the

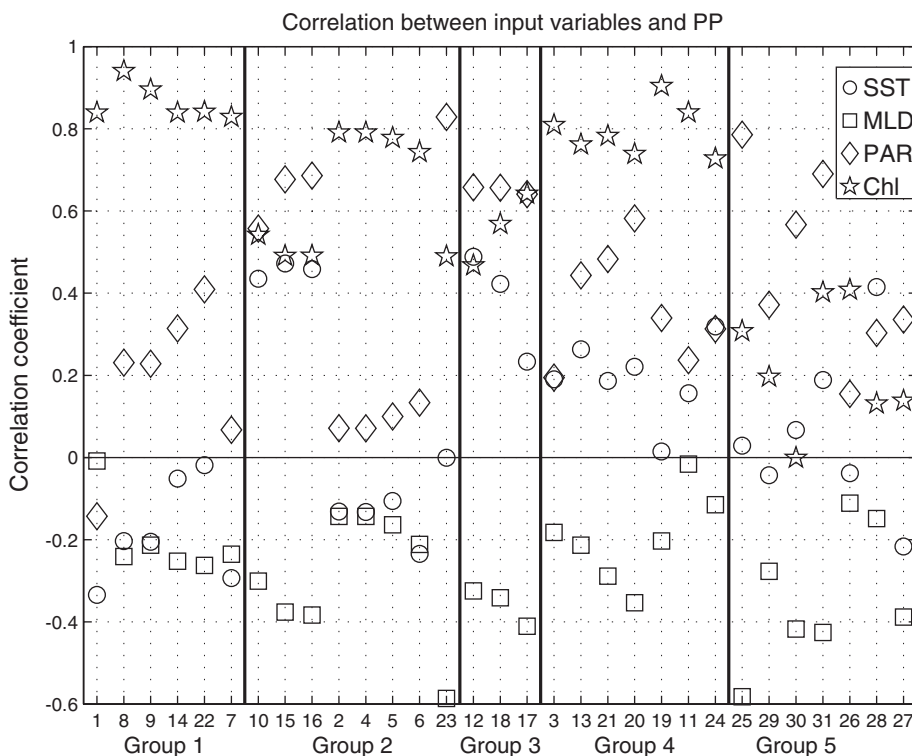


Fig. 19. Pair-wise correlation between modeled primary production and the input variables SST, mixed-layer depth, PAR, and chlorophyll for the months of January and July 1998.

negative correlation between mixed-layer depth and PP is directly proportional to the positive correlation with PAR.

In summary, PP from Group 1 is very highly correlated with chlorophyll concentration, weakly correlated with PAR, and negatively correlated with mixed-layer depth and SST. Group 2 can be divided into two groups. In models #10, 15, 16, and 23, PP is comparably correlated with chlorophyll concentration and PAR, and negatively correlated with mixed-layer depth. The remainder of Group 2 are most highly correlated with chlorophyll and are uncorrelated to PAR. Group 3 estimates of PP show similar relationships as models #10, 14, and 15. PP estimates from Group 4 are, like Group 1, highly correlated to chlorophyll, but unlike Group 1, are also positively correlated with PAR and SST. In principle, Group 5 PP estimates are completely independent of the PPARR3 input fields since only two models used them. Therefore, correlations were generally weaker than with the ocean-color-based models. Even so, PAR explains most of the modeled variability in PP, especially in #25, 30 and 31, while the highest correlation with chlorophyll is $r \sim 0.4$

(#31, which assimilates SeaWiFS, and 26). Mixed-layer depth is consistently negatively correlated (at $r = 0.6$ for #25) and SST is uncorrelated except for #28 ($r = 0.4$).

4. Discussion and conclusions

4.1. Implications of model similarity and divergence

Global PP estimates from the twenty-four ocean-color-based models range over a factor of two (Fig. 5A), from values less than 40 Gt C y^{-1} (models #14, 6, and 12) to those exceeding 60 Gt C y^{-1} (#15, 17, 13, and 21). HYR variants include the lowest and highest global estimates. VGPM variants tend to be average or low, HYR variants and WIDR can be high or low, and WRDR tend to be average or high. VGPM variants that use a variant of the sixth-order polynomial expression tend to be low because they estimate lower PP rates for SST exceeding 20°C , which cover a considerable area of the world ocean ($\sim 60\%$, Table 3).

Presenting model results as a function of deviation from the mean model seems to imply that the

mean is inherently better. We do not believe this to be the case; there is no way to quantify model performance without comparing the output to in situ data (part 3, Friedrichs et al., in preparation). We propose instead that the conditions or regions for which the models differ are those for which it is more difficult to model photosynthesis. For example, model output converges more in regions which have provided more data for model development (Fig. 7, Table 4) and those which do not present HNLC conditions. The most difficult regions are poleward of 40° in all basins, the equatorial region, and northern subtropical Indian Ocean. This results from differences in model output for high chlorophyll concentrations and for extreme SST values (<10°C and >20°C).

The Southern Ocean is unquestionably the most challenging large basin. Two models and a variant (#8/9 and 24) were formulated for the Southern Ocean and parameterized solely with Southern Ocean data. PP estimated by models #8 and 24 is lower than that of the mean model (Fig. 7). However, PP from model #9, which aims to correct the chlorophyll determination in this region, and #19, which also included Southern Ocean data in its formulation and parameterization, are 20–50% larger than the mean (Fig. 7).

The model anomalies are summarized in Table 4. Anomalous models in Group 1 tend to overestimate PP in the Southern Ocean, and under low temperature and high chlorophyll conditions. Group 1 generally produces low PP (except for eutrophic conditions, Figs. 8 and 9) and is highly correlated to the chlorophyll fields (Fig. 19). Group 2 estimates of PP tend to be higher than average; the anomalous models generally overestimate PP in the Southern Ocean, while underestimating PP for SST < 0°C and overestimating it for 10°C > SST < 20°C and in mesotrophic waters (Table 4, Figs. 8 and 10). This group includes the standard VGPM and most variants for which maximum photosynthetic rates occur at or below 20°C (Fig. 18). PP estimated by four of the models in this group (#10, 15, 16, and 23, a WIDI, two WIDR and a WRDR) is more correlated to PAR than to chlorophyll, while the remaining four are correlated only to chlorophyll concentration (Fig. 19). PP estimated by Group 3 tends to be low, except for model #17 (Fig. 5). Group 3 models are quite anomalous compared to the mean, with a tendency to underestimate PP in the Southern Ocean and under conditions of low temperature (<10°C), and to overestimate PP in

the equatorial region (Table 4). The group average model is generally low compared to the mean except in oligotrophic waters (Figs. 6, 8, and 10). These models are more or equally correlated to PAR than to chlorophyll (Fig. 19). Models in Group 4 tend to overestimate PP compared to the mean model (Fig. 5). PP is high particularly in mesotrophic and oligotrophic waters and for SST exceeding 20°C. All of these models include an exponential function of SST (Fig. 15). The global PP fields are highly correlated with chlorophyll concentration and, in some cases with PAR and, unlike in Group 1, positively if weakly correlated with SST (Fig. 19).

Finally, Group 5 estimates of PP were comparable to those of the ocean-color-based models (Fig. 5). They tend to overestimate PP in the Southern Ocean, in the equatorial region, and at SST less than 10°C and over 20°C, and to underestimate high chlorophyll concentrations (Table 4). The GCM-based model fields are weakly related to the input fields, except for #25, 30, and 31, which are correlated with PAR at $r \geq 0.6$, and #25, which is negatively correlated with mixed-layer depth ($r = -0.6$; Fig. 19). Some of the GCM-based models restore nutrients to climatology at depth, which in some comparison studies can increase global production by $\sim 10 \text{ Gt C y}^{-1}$.

Not surprisingly, the parameterization of the maximum or optimal photosynthetic rate has large impact on the variability of the ocean-color-based models and consequently on the relationship groups. Specifically the results of the sensitivity analysis show that the sensitivity to SST perturbations, regardless of model complexity, helps explain the observed dendrogram (Figs. 16 and 4). The large divergence in response to SST perturbations illustrates the need to improve our understanding, and ability to model, the effect of temperature on photosynthesis.

4.2. Strategy for model improvement

Ocean-color-based modeling of primary production is an active area of research, and new models are under development. Ongoing efforts strive to include more data, from a broader geographic range and for more diverse conditions, and to improve model formulation and parameterization. Global estimation of primary production from ocean color requires extrapolating sparse point measurements. Aspects of the photosynthetic process and of the environmental conditions (e.g., light or nutrients)

are parameterized as a function of either biogeography and/or one or more variables which can be measured from spaceborne sensors. The problem is data limited by the amount of (1) representative in situ measurements and (2) satellite-accessible information. Strategies which combine remotely-sensed variables with historical or modeled information that can be linked to geography, biome, or regime are compelling as they hopefully include the best of both worlds.

Complex models are computer-intensive although shortcuts can be made via look-up tables or using simplifying assumptions. The advantage of complex models is that the photosynthetic process is represented with greater fidelity and detail, which allows for greater subtlety in the forcing fields. As more in situ data, or improved satellite data (such as information on nutrient fields, phytoplankton size class or functional groups, or photoadaptive state), become available they can be exploited within most of the existing complex formulations.

The advantage of simple models is that they are very easily implemented. The simplest model examined (#1), a simple function of chlorophyll concentration, estimates consistent global and regional averages production (Fig. 5A). However, this model cannot reflect temporal or spatial variability that does not impact the chlorophyll concentration, including for example, the absence of light. Seasonal variability is underestimated compared to the other models (best seen in Fig. 13) and interannual variability is also less than average (Fig. 5B). Model #1 also overestimates PP in conditions of low PAR or very low SST, and consequently at high latitudes (Figs. 7, 11, and 13). Models that incorporate PAR or SST generate seasonal and temporal variability that is indistinguishable from that of complex models. However, simple parameterizations are more likely to be biased by the data used in the formulation. Competing processes, such as for example the photosynthetic response to temperature versus the correlation between temperature and nutrient content, can easily be confounded or canceled out, especially when limited input data are available to parameterize the processes.

Ocean-color-based models need to resolve variability in addition to average values. Siegel et al. (2001) compared ten PP models (of varied complexity, including WRDR) with a six-year time series of PP and bio-optical measurements at the subtropical Bermuda Atlantic Time Series (BATS) site. PP

models explained ~30% of the observed variance. The best models in reproducing the mean were unable to capture the variability. They concluded that the assumptions of steady state and balanced growth inherent to bio-optical PP models cannot reproduce the unsteady disturbed environment of cells in the ocean.

When asked what is needed to improve model performance, all model developers coincide in requesting more data, ideally together with ancillary data such as nutrients and community structure. An improved understanding of the photosynthetic process requires measurement of the photosynthetic parameters in addition to that of primary production. Data are especially limited from the Southern Ocean, the subtropics, HNLC regions, and the coastal ocean. Initial results for the equatorial Pacific indicate that the community models are improving compared to PPARR2: mismatch with in situ data on the equator decreased by over a factor of two (Friedrichs et al., in prep). Specific concerns for future progress include improved formulation of the quantum yield and of the light field, and more data on the vertical distribution of chlorophyll. Comparisons with in situ data invariably bring up the limitations of discrete ^{14}C uptake measurements (e.g., Richardson et al., 1984). Our strategy is based on ^{14}C measurements because of data density, but thought should be placed on the use of alternate estimates of photosynthetic rate, such as oxygen production (e.g., Bender et al., 2000).

As in PPARR1/2, the PPARR3 modeling exercise includes comparison with in situ data, necessary to quantify model performance (Friedrichs et al., in prep). Parts 1 and 2 presented here provide an unprecedented understanding of the observed similarity among the models and of the conditions under which they perform differently. The large number of participating ocean color and GCM-based models provides an expanded perspective on the range of model performance. We have found that the form in which SST is used impacts the relationship between model output. Future plans include a more comprehensive in situ comparison, including coastal regions, the Southern Ocean, Arabian Sea, and a more detailed examination of temporal variability in subtropical regions (i.e. the Bermuda and Hawaii time series stations). As in PPARR3, we anticipate model development and refinement, and hope to perform ongoing comparison of model performance, such as shown here, independently of the in situ data.

Acknowledgments

We thank Tony Lee of JPL and Stephen Yeager and Scott Doney (now at WHOI) of NCAR for generously providing modeled fields of mixed-layer depth. We are grateful to the SeaWiFS Science Project for the SeaWiFS data set and to the NOAA/NASA AVHRR Pathfinder project for SST, made available by the JPL-PODAAC. We thank two anonymous reviewers for helpful comments that improved an earlier version. Funding was provided by the NASA Ocean Biogeochemistry Program within the Carbon Cycle Science Program. The research described in this paper was carried out at the Jet Propulsion Laboratory, California Institute of Technology, under a contract with the National Aeronautics and Space Administration.

Appendix

Model #1: This model estimates PP as $\sqrt{\text{chl}}$ (Eppley et al., 1985). It ignores any external forcing or changes in physiological state. While other models introduce complexity from geography or forcing fields, this model assumes that the standing stock is sole determinant of photosynthetic rate. All biomass performs identically.

Models #2/3/4: The vertically generalized production model (VGPM) developed by Behrenfeld and Falkowski (1997a) is one of the most widely known and used WIDI PP models. The maximum observed photosynthetic rate within the water column, $P_{\text{opt}}^{\text{B}}$, is obtained as a seventh-order polynomial of SST. Companion model #3 only differs from #2 in that $P_{\text{opt}}^{\text{B}}$ is estimated as an exponential function of temperature following Eppley (1972). Model #4 is identical to Model #2, but was run independently as a former standard MODIS PP product.

Model #5: This VGPM variant estimates the total integrated chlorophyll concentration from a continuous function (Morel and Berthon, 1989) rather than in two steps as in Model #2; the euphotic depth (attenuation coefficient) is defined following Morel and Maritorena (2001).

Model #6: This VGPM variant formulates $P_{\text{opt}}^{\text{B}}$ as a function of SST and chlorophyll concentration (Kameda and Ishizaka, in press). The model is based on the assumptions that changes in chlorophyll concentration depend on the abundance of large phytoplankton and that chlorophyll-specific productivity is inversely proportional to phytoplankton size.

Model #7: This VGPM defines $P_{\text{opt}}^{\text{B}}$ by multiplying a theoretical maximum $P_{\text{opt}}^{\text{B}}$ by nutrient and light limitation factors obtained from a globally-run ecosystem model (Moore et al., 2002ba). It assumes that $P_{\text{opt}}^{\text{B}}$ depends more on available nutrients and light than on SST.

Models #8/9: This VGPM variant was developed for the Southern Ocean and was only run south of 50°S (Dierssen and Smith, 2000; Dierssen et al., 2000). It uses the average $P_{\text{opt}}^{\text{B}}$ measured in the study area, as no relationship was found between environmental observations and $P_{\text{opt}}^{\text{B}}$. Model #8 uses the standard chlorophyll concentration as input. #9 answers the challenges to satellite determination of chlorophyll in the Southern Ocean by transforming the SeaWiFS value with an empirical relationship observed between ocean color and in situ measurements.

Model #10: This model is based on the formulation obtained through dimensional analysis by Platt and Sathyendranath (1993). The photosynthetic parameters ($P_{\text{max}}^{\text{B}}$ and the photo-acclimation parameter E_k) are assigned by combining a temperature-dependent relationship for the maximum growth rate (Eppley, 1972) with dynamic provinces derived from fuzzy logic (as in Moore et al., 2001) to retrieve the carbon to chlorophyll ratio following the empirical relation of Cloern et al. (1995). Primary production is integrated to the mixed-layer depth.

Model #11: This model is the standard Howard, Yoder, Ryan (HYR) model (Howard and Yoder, 1997). Maximum growth rate is parameterized as a function of SST according to Eppley (1972). Primary production is integrated to the mixed-layer depth rather than to the euphotic depth.

Model #12: This HYR variant uses mixed-layer depth information to quantify the photoadaptive variables within the euphotic zone, as well as to address water column partitioning of primary production relative to euphotic depth.

Model #13: This HYR variant integrates photosynthesis to the euphotic depth as defined in Behrenfeld and Falkowski (1997a) rather than to the mixed-layer depth (Carr, 2002).

Model #14: This model uses an artificial neural network to perform a generalized nonlinear regression of PP on several predictive variables, including latitude, longitude, day length, mixed-layer depth, SST, $P_{\text{opt}}^{\text{B}}$ (computed according to the VGPM), PAR, and surface chlorophyll (Scardi, 2000, 2001). Since there are insufficient data to calibrate the

neural network on a global scale, PP values from other models (VGPM, HYR, and the MOD-27 formulation (Esaias, 1996)) were considered measurements where there were none.

Models #15/16/17: These three models are WIDR models. Model #14 uses Behrenfeld and Falkowski (1997a) to estimate $P_{\text{opt}}^{\text{B}}$. The surface spectral irradiance, estimated with Gregg and Carder (1990), is used to obtain a spectrally weighted depth-averaged light attenuation coefficient within the mixed layer. Surface irradiance is converted from cosine to scalar. Companion model #15, in contrast, does not convert the irradiance from cosine to scalar. Model #16 differs from #14 by using the $P_{\text{max}}^{\text{B}}$ function from Antoine and Morel (1996).

Model #18: This WIDR model estimates depth-dependent photosynthesis as a function of chlorophyll concentration, temperature, and PAR. The depth-distribution of PAR is determined by surface chlorophyll concentration while the depth-distribution of chlorophyll is given by the PAR profile and the surface chlorophyll concentration. The carbon fixation rate is empirically estimated as a function of PAR and temperature (Asanuma et al., 2003).

Model #19: This WIDR model is based on chlorophyll-specific phytoplankton absorption, which is parameterized empirically as a function of SST (Marra et al., 2003). Absorption by photosynthetic pigments is distinguished from total absorption; the former is used to calculate productivity and the latter is used to estimate light attenuation in the water column. The quantum efficiency is obtained from a hyperbolic tangent and a constant ϕ_{max} . The depth profile of chlorophyll is estimated assuming a gaussian shape with parameters determined by the surface value. The attenuation coefficient of chlorophyll is also SST-dependent.

Model #20: This WRDR model (Morel, 1991) is based on measurements of photosynthesis versus irradiance and is formulated using chlorophyll-specific wavelength-resolved absorption and quantum yield. Temperature dependence is given by the parameterization of $P_{\text{max}}^{\text{B}}$ which follows Eppley (1972). The chlorophyll profile is determined to be well-mixed or stratified according to the ratio of mixed-layer depth and the euphotic depth, and if stratified, assigned a gaussian profile as in Morel and Berthon (1989). Mean photo-physiological parameters are from Morel et al. (1996). The model is run in its 'satellite' version (Antoine et al., 1996), where PP is the product of integral biomass, the

daily irradiance, and ψ^* (the cross-section of algae for photosynthesis per unit of areal chlorophyll biomass). Lookup tables for ψ^* were previously generated using the full WRDR model, and are used to increase computational efficiency.

Model #21: This model is an implementation of the Morel (1991) WRDR model in which the depth distribution of chlorophyll is assumed constant throughout the water column. The broadband incident PAR is spectrally resolved using a lookup-table generated from a single run of the Gregg and Carder (1990) marine irradiance model where the effects of clouds and aerosols are essentially linearly scaled. The model uses 60-min time and 10-m depth steps at 5-nm wavelength resolution when run using the global datasets.

Model #22: This WRDR follows the model of Platt and Sathyendranath (1988) as implemented at global scale by Longhurst et al. (1995). It uses biogeographical provinces to define the values of the parameters to describe the light-photosynthesis curve and the chlorophyll depth profile. Photosynthetic parameters were updated using an extended data set provided by the Bedford Institute of Oceanography and an extensive literature review. Spectral surface irradiance is first estimated independently with the model of Gregg and Carder (1990) combined with a correction for cloud cover and then scaled to match the PAR values provided for the exercise. Spectral light is subsequently propagated in the water column with a bio-optical model with updated parameterizations of the inherent optical properties. All changes to the original implementation of Longhurst et al. (1995) are detailed by Mélin (2003).

Model #23: This WRDR model derives spectral irradiance from the PAR using Tanré et al. (1990). Quantum yield is parameterized from a maximum value and a light dependent term (Waters et al., 1994; Bidigare et al., 1992). The chlorophyll profile is assumed vertically uniform. A sigmoidal temperature dependence was applied to the maximum quantum yield, based on a vertical profile of temperature derived from SST and mixed-layer depth.

Model #24: This WRDR was developed for the Southern Ocean (Arrigo et al., 1998), but has been applied to the global fields in this study. It is based on spectrally varying chlorophyll absorption and a scaling of the photo-acclimation parameter E_k to the daily mean irradiance. The rate of production is determined by temperature and by light limitation.

Chlorophyll is assumed uniform in the mixed layer and decreases exponentially at greater depths.

Model #25: The Pelagic Interactions Scheme for Carbon and Ecosystem Studies (PISCES) ocean biogeochemistry model has three nutrients (Fe, P, and Si), and two size classes each of phytoplankton and zooplankton, as well as detritus and semi-labile dissolved organic matter (Aumont et al., 2003; Bopp et al., 2003). PISCES is coupled online to the OPA general circulation model (Madec et al., 1998). OPA has a horizontal resolution of 2° ; the latitudinal resolution is enhanced to 0.5° at the equator and the pole. It resolves 30 vertical levels at 10-m intervals in the top 100 m. It is forced with daily averaged values of winds and fluxes from the National Centers for Environmental Prediction (NCEP) reanalysis.

Model #26: This ecosystem model (Moore et al., 2002a,b) has four nutrients (nitrogen, phosphorus, silicon, and iron) and three phytoplankton groups (diatoms, diazotrophs, and a generic small phytoplankton class). Growth rates can be limited by available nutrients and/or light levels. The diatoms can also be limited by silicon and the diazotrophs are not nitrogen-limited. This model is run as multiple 1-D mixed layer models, forced here by the provided mixed-layer depth.

Model #27: This 11-compartment North Pacific Ecosystem Model Used for Regional Oceanography (NEMURO), developed by the North Pacific Marine Science Organization (Eslinger et al., 2000), has two size classes each of phytoplankton and zooplankton, and two nutrients: nitrate and silicate. The coupled GCM and ecosystem model is described by Aita et al. (2003). The horizontal resolution is 1 by 1° over a global domain not including the Arctic Ocean.

Model #28: This biogeochemical model estimates new production by restoring surface nitrate to the monthly World Ocean Atlas 2001 data synthesis (<http://www.nodc.noaa.gov/OC5/WOA01/pr-woa01.html>) and then applies a spatially dependent f-ratio to obtain primary production. Climatological forcing was used.

Model #29: This PISCES model variant, PISCES-T, has improved parameterization of meso-zooplankton growth and mortality rates, and a temperature-dependent degradation of particulate organic matter (Buitenhuis et al., 2006). As in #25, it is coupled to the OPA and is forced by NCEP reanalysis. This model version does not restore to climatological nutrients below the mixed layer.

Model #30: The NASA Ocean Biogeochemical Model (NOBM) simulates four phytoplankton groups (diatoms, chlorophytes, cyanobacteria, and coccolithophores) and four nutrients (nitrate, ammonium, silica, and iron) (Gregg et al., 2003). The model is approximately 0.8° resolution with 14 vertical layers in quasi-isopycnal configuration. The model was forced by monthly mean winds and shortwave radiation from NCEP for 1998 and 1999.

Model #31: In this NOBM variant SeaWiFS chlorophyll data were assimilated for 1998 and 1999. Assimilation occurred on a daily basis, using the Conditional Relaxation Analysis Method (Oort, 1983). The assimilation affected the model representations of total chlorophyll (sum of the four phytoplankton groups), but not the individual community distributions directly. Primary production was affected by the change in total chlorophyll, as well as by indirect effects such as subsurface irradiance resulting from absorption and scattering by the changed chlorophyll field.

References

- Aita, M.N., Yamanaka, Y., Kishi, M.J., 2003. Effect of ontogenetic vertical migration of zooplankton on the results of NEMURO embedded in a general circulation model. *Fisheries Oceanography* 12, 284–290.
- Antoine, D., Morel, A., 1996. Oceanic primary production 2. Adaptation of a spectral light-photosynthesis model in view of application to satellite chlorophyll observations. *Global Biogeochemical Cycles* 10, 43–55.
- Antoine, D., Andre, J.-M., Morel, A., 1996. Oceanic primary production 2. Estimation at global scale from satellite (Coastal Zone Color Scanner) chlorophyll. *Global Biogeochemical Cycles* 10, 57–69.
- Arrigo, K.R., Worthern, D., Schnell, A., Lizotte, M.P., 1998. Primary production in Southern Ocean waters. *Journal of Geophysical Research* 103, 15587–15600.
- Asanuma, I., Nieke, J., Matsumoto, K., Kawano, T., 2003. Optical properties control primary productivity model on the East China Sea. In: Frouin, J.R. (Ed.), *Ocean Remote Sensing and Applications*, vol. 4892. SPIE, pp. 312–319.
- Aumont, O., Maier-Reimer, E., Blain, S., Pondaven, P., 2003. An ecosystem model of the global ocean including Fe, Si, P colimitations. *Global Biogeochemical Cycles* 17, doi:10.1029/2001GB001745.
- Behrenfeld, M., Falkowski, P., 1997a. Photosynthetic rates derived from satellite-based chlorophyll concentration. *Limnology and Oceanography* 42 (1), 1–20.
- Behrenfeld, M., Falkowski, P., 1997b. A consumer's guide to phytoplankton primary productivity models. *Limnology and Oceanography* 42 (7), 1479–1491.
- Bender, M., Dickson, M.-L., Orchardo, J., 2000. Net and gross production in the Ross Sea as determined by incubation

- experiments and dissolved O₂ studies. *Deep Sea Research II* 47, 3141–3158.
- Berger, W.H., 1989. Global maps of primary productivity. In: Berger, W.H., Smetacek, V.S., Wefer, G. (Eds.), *Productivity of the Ocean: Present and Past*. Wiley, Berlin, pp. 429–455.
- Bidigare, R.R., Prézélin, B.B., Smith, R.C., 1992. Bio-optical models and the problems of scaling. In: *Primary Productivity and Biogeochemical Cycles in the Sea*. Plenum Press, New York, pp. 175–212.
- Bopp, L., Kohfeld, K., Le Quéré, C., Aumont, O., 2003. Dust impact on marine biota and atmospheric CO₂ during glacial periods. *Paleoceanography* 18, 10.1029/2002PA000810.
- Buitenhuis, E.T., Le Quéré, C., Aumont, O., Beaugrand, G., Bunker, A., Hirst, A., Ikeda, T., O'Brien, T., Piontkovski, S., Straile, D., 2006. Biogeochemical fluxes through mesozooplankton. *Global Biogeochemical Cycles* 20 (2), GB2003.
- Campbell, J., Antoine, D., Armstrong, R., Balch, W., Barber, R., Behrenfeld, M., Bidigare, R., Bishop, J., Carr, M.-E., Esaias, W., Falkowski, P., Hoepffner, N., Iverson, R., Kiefer, D., Lohrenz, S., Marr, J., Morel, A., Ryan, J., Vedernikov, V., Waters, K., Yentsch, C., Yoder, J., 2002. Comparison of algorithms for estimating ocean primary production from surface chlorophyll, temperature, and irradiance. *Global Biogeochemical Cycles* 16(3), 10.1029/2002GL015068.
- Carr, M.-E., 2002. Estimation of potential productivity in Eastern Boundary Currents using remote sensing. *Deep-Sea Research II* 49, 59–80.
- Cloern, J.E., Grenz, C., Videgar-Lucas, L., 1995. An empirical model of the phytoplankton chlorophyll:carbon ratio—the conversion factor between productivity and growth rate. *Limnology and Oceanography* 40, 1313–1321.
- Dierssen, H., Smith, R.C., 2000. Bio-optical properties and remote sensing ocean color algorithms for Antarctic Peninsula waters. *Journal of Geophysical Research* 105 (C), 26301–26312.
- Dierssen, H., Vernet, M., Smith, R.C., 2000. Optimizing models for remotely estimating primary production in Antarctic coastal waters. *Antarctic Science* 12, 20–32.
- Eppley, R.W., 1972. Temperature and phytoplankton growth in the sea. *Fisheries Bulletin* 70, 1063–1085.
- Eppley, R., Steward, E., Abbott, M., Heyman, U., 1985. Estimating ocean primary production from satellite chlorophyll: introduction to regional differences and statistics for the Southern California Bight. *Journal of Plankton Research* 7, 57–70.
- Esaias, W., 1996. MODIS algorithm theoretical basis document for product MOD-27: ocean primary productivity. WWW Page (<http://modis.gsfc.nasa.gov/data/atbd/atbd-mod24.pdf>).
- Eslinger, D.V., Kashiwai, M.B., Kishi, M.J., Megrey, B.A., Ware, D.M., Werner, F.E., 2000. Final report of the international workshop to develop a prototype lower trophic level ecosystem model for comparison of different marine ecosystems in the north Pacific. *PICES Scientific Report* 15, 1–77.
- Field, C., Behrenfeld, M., Randerson, J., Falkowski, P., 1998. Primary production of the biosphere: integrating terrestrial and oceanic components. *Science* 281 (5374), 237–240.
- Friedrichs, M.A.M., Carr, M.-E., Barber, R., Schmeltz, M., Gentili, B., Morel, A., Arrigo, K.R., Reddy, T., Asanuma, I., Behrenfeld, M., Bidigare, B., Ciotti, A., Dierssen, H., Dowell, M., Dunne, J., Esaias, W., Turpie, K., Hoepffner, N., Melin, F., Ishizaka, J., Le Quéré, C., Aumont, O., Marra, J., Moore, K., Ryan, J., Scardi, M., Smyth, T., Groom, S., Tilstone, G.H., Waters, K., Yamanaka, Y., in preparation. Comparison of primary production estimates in the tropical Pacific Ocean, in preparation.
- Gregg, W., Carder, K., 1990. A simple spectral solar irradiance model for cloudless maritime atmospheres. *Limnology and Oceanography* 35, 1657–1675.
- Gregg, W.W., Ginoux, P., Schopf, P., Casey, N., 2003. Phytoplankton and iron: validation of a global three-dimensional ocean biogeochemical model. *Deep-Sea Research II* 50, 3143–3169.
- Howard, K.L., Yoder, J.A., 1997. Contribution of the subtropical oceans to global primary production. In: Liu, C.-T. (Ed.), *Space Remote Sensing of Subtropical Oceans*. vol. COSPAR Colloquia Series, vol. 8. Proceedings of COSPAR Colloquium on Space Remote Sensing of Subtropical Oceans, Taiwan. Pergamon, New York, pp. 157–168.
- Kameda, T., Ishizaka, J., in press. Size-fractionated primary production estimated by a two-phytoplankton community model applicable to ocean color remote sensing. *Journal of Oceanography*, in press.
- Koblentz-Mishke, O.I., Volkovinsky, V.V., Kabanova, Y.G., 1970. Plankton primary production of the world ocean. In: Wooster, W. (Ed.), *Scientific Exploration of the South Pacific*. National Academy of Sciences, Washington, DC, pp. 183–193.
- Le Borgne, R., Barber, R., Delcroix, T., Inoue, H., Mackey, D., Rodier, M., 2002. Pacific warm pool and divergence: temporal and zonal variations on the equator and their effects on the biological pump. *Deep-Sea Research* 49 (13–14), 2471–2512.
- Longhurst, A., Sathyendranath, S., Piatt, T., Caverhill, C., 1995. An estimate of global primary production in the ocean from satellite radiometer data. *Journal of Plankton Research* 17, 1245–1271.
- Madec, G., Delecluse, P., Imbard, M., Levy, C., 1998. OPA 8.1. Ocean General Circulation Model Reference Manual. IPSL Notes du pôle de modélisation, Note 11.
- Marra, J., Ho, C., Trees, C., 2003. An alternative algorithm for the calculation of primary productivity from remote sensing data. LDEO Technical Report #LDEO-2003-1.
- McClain, C.R., Cleave, M.L., Feldman, G., Gregg, W., Hooker, S., Kuring, N., 1998. Science quality SeaWiFS data for global biosphere research. *Sea Technology* 39, 10–16.
- Mélin, F., 2003. Potentiel de la télédétection pour l'analyse des propriétés optiques du système océan-atmosphère et application à l'estimation de la photosynthèse phytoplanktonique. Ph.D., Université Paul Sabatier, Toulouse, France, unpublished.
- Middleton, G.V., 2000. *Data Analysis in the Earth Sciences Using MATLAB*. Prentice-Hall, Englewood Cliffs, NJ.
- Moore, J.K., Doney, S.C., Glover, D.M., Fung, I.Y., 2002a. Iron cycling and nutrient-limitation patterns in surface waters of the world ocean. *Deep-Sea Research II* 49, 463–507.
- Moore, J.K., Doney, S.C., Kleypas, J.A., Glover, D.M., Fung, I.Y., 2002b. An intermediate complexity marine ecosystem model for the global domain. *Deep-Sea Research II* 49, 403–462.
- Moore, T.S., Campbell, J., Feng, H., 2001. A fuzzy logic classification scheme for selecting and blending satellite ocean color algorithms. *IEEE Transactions on Geoscience and Remote Sensing* 39 (8), 1764–1776.

- Morel, A., 1991. Light and marine photosynthesis: a spectral model with geochemical and climatological implications. *Progress in Oceanography* 26, 263–306.
- Morel, A., Berthon, J.F., 1989. Surface pigments, algal biomass profiles, and potential production of the euphotic layer: relationships reinvestigated in view of remote-sensing applications. *Limnology and Oceanography* 34 (8), 1545–1562.
- Morel, A., Antoine, D., Babin, M., Dandonneau, Y., 1996. Measured and modeled primary production in the northeast Atlantic (EUMELI JGOFS program): the impact of natural variations in photosynthetic parameters on model predictive skill. *Deep-Sea Research I* 43, 1273–1304.
- Morel, A., Maritorena, S., 2001. Bio-optical properties of oceanic waters: A reappraisal. *Journal of Geophysical Research* 106, 7163–7180.
- Ondrusek, M.E., Bidigare, R.R., Waters, K., Karl, D.M., 2001. A predictive model for estimating rates of primary production in the subtropical north Pacific Ocean. *Deep-Sea Research II* 48 (8–9), 1837–1863.
- Oort, A.H., 1983. Global atmospheric circulation statistics, 1958–1973. NOAA Professional Paper 14.
- Platt, T., Sathyendranath, S., 1988. Oceanic primary production: estimation by remote sensing at local and regional scales. *Science* 241, 1613–1620.
- Platt, T., Sathyendranath, S., 1993. Estimators of primary production for interpretation of remotely sensed data on ocean color. *Journal of Geophysical Research* 98, 14561–14567.
- Richardson, K., Samelsson, G., Hallgren, J., 1984. The relationship between photosynthesis measured by C-14 incorporation and by uptake of inorganic carbon in unicellular algae. *Journal of Experimental Marine Biology and Ecology* 81 (3), 241–250.
- Rohlf, F.J., 1963. Classification of *Aedes* by numerical taxonomic methods (Diptera: Culicidae). *Annals of the Entomological Society of America* 56, 798–804.
- Scardi, M., 2000. Neuronal network models of phytoplankton primary production. In: Lek, S.G.J.-F. (Ed.), *Artificial Neuronal Networks: Application to Ecology and Evolution*. Springer, Berlin/Heidelberg, pp. 115–129.
- Scardi, M., 2001. Advances in neural network modeling of phytoplankton primary production. *Ecological Modelling* 146, 33–45.
- Siegel, D., Westberry, T., O'Brien, M., Nelson, N., Michaels, A., Morrison, J., Scott, A., Caporelli, E., Sorensen, J., Maritorena, S., Garver, S., Brody, E., Ubante, J., Hammer, M., 2001. Bio-optical modeling of primary production on regional scales: the Bermuda BioOptics project. *Deep-Sea Research II* 48, 1865–1896.
- Tanré, D., Deroo, C., Duhaut, P., Herman, M., Morcrett, J., Perbos, J., Deschamps, P., 1990. Description of a computer code to simulate the satellite signal in the solar spectrum. *International Journal of Remote Sensing* 11, 659–668.
- Waters, K., Smith, R., Marra, J., 1994. Phytoplankton production in the Sargasso Sea as determined using optical mooring data. *Journal of Geophysical Research* 99, 18385–18402.